10.1098/rspa.2002.1063

THE ROYAL SOCIETY

Acoustic resonances in the bubble plume formed by a plunging water jet

By Thomas R. Hahn[1], Thomas K. Berger[1] and Michael J. Buckingham[1,2]

[1]*Marine Physical Laboratory, Scripps Institution of Oceanography, University of California, San Diego, 9500 Gilman Drive, La Jolla, CA 92093-0238, USA*

[2]*Institute of Sound and Vibration Research, University of Southampton, Southampton SO17 1BJ, UK*

Received 23 November 2001; accepted 21 August 2002; published online 16 May 2003

Experiments were performed to investigate the near-field sound from an axisymmetric conical bubble plume formed by a continuous vertical freshwater jet as it penetrates the surface of a pool of fresh water. The volume fluxes of the air and water entering the pool were carefully controlled and monitored during the experiments and a hydrophone detected the acoustic pressure field adjacent to the plume at frequencies between 100 Hz and 1 kHz. Up to five non-uniformly spaced peaks were observed in the pressure spectrum. These spectral peaks are due to coherent collective oscillations of the bubbles within the plume, that is to say, the biphasic bubbly medium behaves as a continuum, acting as a resonant conical cavity beneath the jet. All the eigenfrequencies were found to exhibit inverse-fractional power-law scalings of the same form, $f_m \propto u_{\mathrm{j}}^{-1/2} q^{-1/4}$, where f_m is the frequency of the mth spectral peak, u_{j} is the jet velocity, q is the air entrainment ratio, that is, the ratio of the air-to-water volume fluxes in the jet, and the unspecified constant shows a nonlinear dependence on m. A two-component theoretical model has been developed for the eigenfrequencies of the plume. From a fluid-dynamics argument based on the conservation of momentum flux in the two-phase flow, the speed of sound within the bubbly medium is shown to increase as the square root of depth in the plume. This is incorporated into an acoustic analysis in which the wave equation is solved analytically, taking account of the cone-like geometry of the bubble-plume cavity, including the near-rigid boundary condition at the penetration depth, where the bubbly region ends abruptly. The resultant expression for the frequencies of the lowest-order longitudinal modes of the bubbly cavity exhibits the inverse-fractional power-law scalings observed in the experiments. The experiments and theory are consistent with the conclusion that the scaling of the eigenfrequencies with the inverse square root of the jet velocity stems from the square-root sound-speed profile within the biphasic plume.

Keywords: acoustic emission; collective bubble oscillations; bubble plume resonances; plunging water jet; two-phase flow

1. Introduction

When a jet of water penetrates the surface of a pool of water, a turbulent region beneath the entry point is created and air in the form of bubbles is entrained. The bubbles are advected longitudinally (downwards) and laterally (outwards) by the turbulence to form a plume of aerated water below the surface. The hydrodynamics of jet-and-plume systems (Bin 1993) is relevant to chemical mixing processes, aeration of fluids and gas transfer across the air–sea interface. Also important, mainly in connection with the production of wind-generated low-frequency (less than 1 kHz) ambient noise in the ocean (Urick 1986), are the acoustic properties of bubble plumes formed by plunging water jets at or near the leading edge of breaking waves.

It is well established that low-frequency wind-driven noise exists in the ocean (Burgess & Kewley 1983; Hollett 1994; Kerman 1984; Wille & Geyer 1984), due to bubbles created by wave breaking. However, the wind-driven component of the low-frequency noise cannot be due to the resonances of individual bubbles, since the bubble sizes required are much larger than those commonly observed in the ocean. An alternative mechanism, suggested independently by Carey & Bradley (1985); Carey & Fitzgerald (1987), Carey & Browning (1988) and Prosperetti (1988*a*,*b*), is that a cloud of bubbles near the ocean surface may, in some sense, oscillate collectively to produce sound at the eigenfrequencies of the cloud, which are considerably lower than the radial resonance frequencies of the individual bubbles constituting the cloud. Support for the collective-oscillation hypothesis is found in the recordings of sound from laboratory-generated breaking waves (Kolaini 1998; Kolaini & Crum 1994; Lamarre & Melville 1994; Loewen & Melville 1994), and also from bubble clouds created in tipping-trough (Carey *et al.* 1993) and bucket-drop (Kolaini *et al.* 1993) experiments.

A more controlled bubble cloud was created in an experiment conducted by Yoon *et al.* (1991), who observed acoustic resonances in a homogeneous cylindrical column of rising bubbles injected by an array of needles at the base of a large water tank. The bubble column acted as a leaky resonant cavity, producing sound in the surrounding water at the frequencies of the longitudinal modes of the column. Although convincing as a source of low-frequency sound, the bubble column differed in several respects from bubble clouds formed in the ocean. A more natural bubble cloud was investigated by Orris & Nicholas (2000), who measured the sound-pressure field in the water surrounding the bubble plume created by a plunging water jet. They observed peaks in the pressure spectrum at frequencies below 1 kHz, which they attributed to the collective oscillation of the bubble plume as a whole.

A bubble plume formed by a plunging water jet provides a canonical system that may be easily produced and carefully controlled in the laboratory, thus allowing its hydrodynamic and acoustic properties to be investigated quantitatively. At the same time, the physics of the system is expected to yield some insight into the acoustic behaviour of bubble plumes occurring in natural bodies of water.

In the first part of this article, a series of experiments is described in which the near-field low-frequency sound pressure from the bubble plume beneath a vertical circular freshwater jet was measured with an omni-directional hydrophone located adjacent to the plume in the surrounding water. The observed pressure spectra exhibit several non-uniformly distributed peaks below 1 kHz, which are associated with resonances of the bubble-plume cavity. The eigenfrequencies depend on the jet velocity, u_{j}, at the

entry point and the air entrainment ratio, q, the latter being defined as the ratio of the air-volume flux to water-volume flux in the jet. Each eigenfrequency scales accurately as $u_{\mathrm{j}}^{-1/2}$, i.e. inversely as the square root of the jet velocity, and approximately as $q^{-1/4}$, i.e. inversely as the fourth root of the air-volume flux entrained by the jet.

These inverse-fractional power-law scalings of the eigenfrequencies in the acoustic spectrum are examined in the second part of the article, in which the external sound field generated by the bubble plume is analysed theoretically on the basis of the hydrodynamic properties of the biphasic flow. An essential part of the argument involves the conservation of the mean downward momentum flux of the turbulence within the plume, a condition that leads to a sound-speed profile down the axis of the bubbly domain that varies as $x^{1/2}$, where x is the depth beneath the entry point of the jet. This square-root form for the longitudinal sound-speed profile is incorporated into the wave equation for the sound field within the conical bubble-plume cavity, which is then solved analytically subject to appropriate boundary conditions. From the solution, an explicit expression for the eigenfrequencies of the plume is derived, which, it turns out, exhibits the same inverse-fractional power-law scalings as found in the data. It is evident, in particular, that the scaling of the eigenfrequencies with $u_{\mathrm{j}}^{-1/2}$ stems from the square-root dependence of the sound-speed profile within the plume.

Part I. Experiments

2. Acoustic experiments

(*a*) *Tank measurements*

The acoustic measurements were made in a non-anechoic powder-coated aluminium tank of area $3 \times 2\,\mathrm{m}^2$ and depth of 1.6 m. The tank was filled with tap water to a depth of 1.55 m, and the level was kept constant using a small surface-skimmer overflow during continuous operation of the jet. A schematic of the experimental set-up is shown in figure 1.

A continuous circular water jet was directed vertically downwards from a size-14-gauge pipetting needle (internal diameter (ID), 1.600 mm; outer diameter, 2.108 mm) onto the free surface of the water. The needles used were at least 60 ID long and were mounted vertically above the water surface at a height that was adjustable with a precision linear-motion device. Jet velocities between 4 and $10\,\mathrm{m\,s}^{-1}$ (the maximum being set by the mains pressure of *ca.* 350 kPa) produced bubble plumes ranging from *ca.* 10 to 20 cm deep.

Precision control of the volumetric flux of air entrained by the jet was achieved by the use of a mixing nozzle (figure 2), designed to emulate the entrainment behaviour of a free-plunging jet. Collar-like nozzles of this type are commonly used to measure the volume of air entrained by plunging jets, with usual values of the collar openings ranging from 1.2 to 3 times the jet diameter (Bin 1993). It is important to note that, in our experiments, the bottom of the collar was kept below the water surface to ensure that all the air injected into the nozzle was entrained by the jet. The entrainment ratio, defined as $q = Q_{\mathrm{a}}/Q_{\mathrm{w}}$, where Q_{a} and Q_{w} are, respectively, the volume fluxes of air and water, was adjustable with the particular nozzle shown in figure 2 within the range $0.4 \leqslant q \leqslant 0.82$. The volume flux of air supplied to the nozzle was precision controlled with a micrometre valve. The temperature and

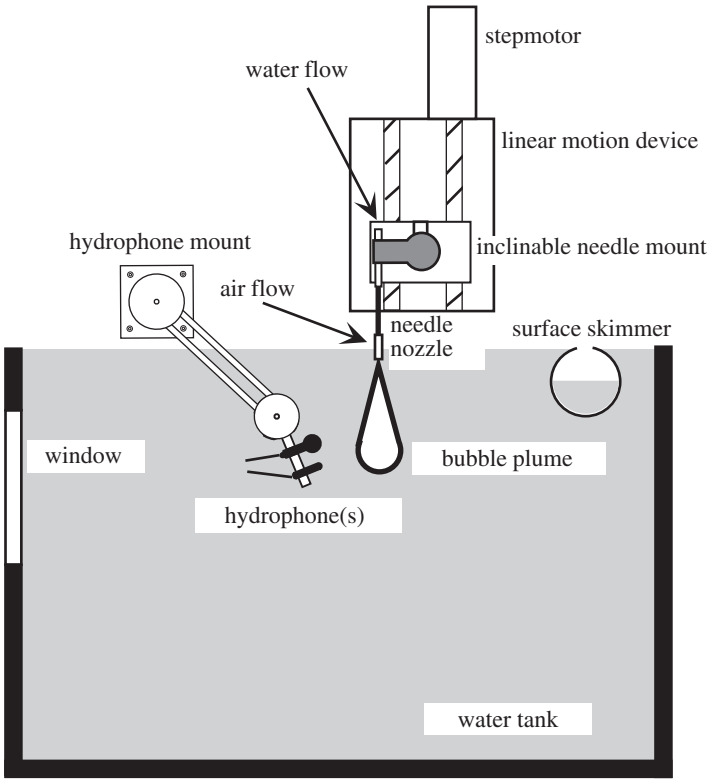

Figure 1. Schematic showing the experimental arrangement for controlling and monitoring the air and water fluxes in the jet, and for detecting the low-frequency acoustic signature of the bubble plume in the tank.

pressure of the air passing through the flowmeters were monitored and the flow rate was corrected to the standard pressure at the entrainment point. For all the datasets reported here, the total error in the measurement of q is less than 5% and in most cases is estimated to be less than 2%.

Two calibrated hydrophones, an ITC 1089D and an ITC 1042, were used to detect the sound-pressure field from the bubble plume at frequencies up to 1 kHz. The hydrophone signals were pre-amplified and digitally sampled at a rate of 4 kHz, and average pressure spectra were computed using a 2048-point fast Fourier transform, yielding a frequency resolution of 2 Hz. At least 390 Hann-windowed spectra were averaged together, representing a 200 s averaging time, to obtain the final spectral estimates of the acoustic pressure from the plume. As a check on the stability of the peaks in the spectrum, the hydrophone was moved relative to the bubble plume, and the eigenfrequencies were observed to remain constant irrespective of the position of the receiver. (The spectral level, of course, varied.)

A broadband source was used to identify the frequencies of the natural resonances of the tank. Provided that the hydrophone was within 10 cm or so of the edge of the plume, the tank resonances were found to be insignificant, having no effect on the spectral peaks from the plume (Hahn 1999). Because the objective of the experiments was to determine the frequencies of these peaks rather than absolute spectral levels, no calibration correction for tank effects was needed or applied.

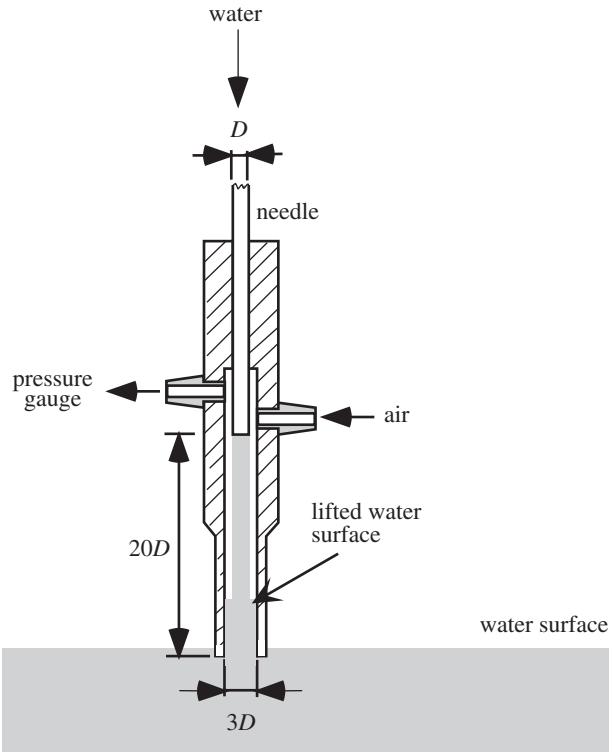

Figure 2. Mixing nozzle with collar used for producing the jet and controlling the volume flux of air entrained in the water. The radius of the nozzle is $R_j = 0.8$ mm, the jet velocities were between 4 and 10 m s^{-1} and the entrainment ratio, q, was in the range 0.4–0.82.

(*b*) *Lake measurements*

As a further check to ensure that the spectral peaks were not artefacts of the tank, the experiments were repeated in a natural body of fresh water, Lake Miramar, some 20 km northeast of La Jolla, CA, in which the water depth is *ca.* 30 m. The set-up on the lake, shown in figure 3, was similar to that in the tank, except that the vertical plunging jet was mounted on a floating platform and no mixing nozzle was used. The nozzle was omitted because wind-driven ripples on the surface of the lake introduced a vertical motion to the platform, making it impossible to maintain the base of the nozzle at a precise depth immediately beneath the surface.

With no mixing nozzle, we were unable to measure directly the amount of air entrained by the jet. In effect, we had a fixed air entrainment ratio that was set by the parameters of the free jet (Bin 1988): with $u_j = 9.5$ m s^{-1} and a jet length approximately 15 times the jet diameter, we inferred that $q \approx 0.9$. Although the jet velocity, u_j, was adjustable, just as in the tank, the functional dependence of the eigenfrequencies on u_j was not pursued in the lake. Having established that, at a fixed u_j, the spectral peaks observed in the lake matched those in the tank, the lake measurements were terminated, largely because the precision achievable in the natural environment was poor, due to platform motion, surface roughness and other factors, compared with the full control and concomitant accuracy available with the laboratory measurements.

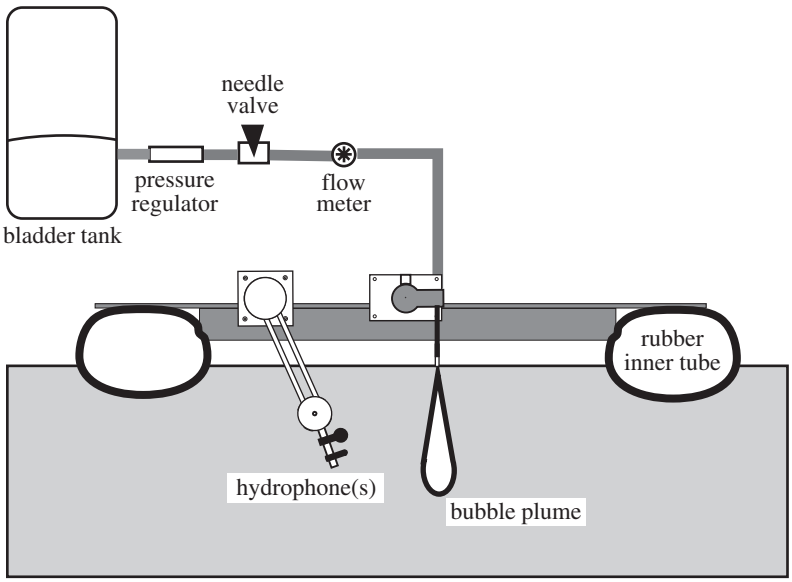

Figure 3. Schematic of the floating platform and experimental set-up used on Lake Miramar. The free vertical jet produced an air entrainment ratio $q \approx 0.9$, with the same range of jet velocities as in the tank experiments.

3. The observed acoustic spectra

Figure 4 shows a representative spectrum of the sound-pressure field generated by the bubble plume in the tank. The most prominent features of the spectrum are the four peaks at 287, 464, 583 and 696 Hz, which are interpreted as corresponding to longitudinal (i.e. depth) modes of oscillation of the resonant cavity formed by the bubble cloud. Modes beyond the fifth are not usually observed in the spectra, probably because of the high attenuation within the bubble plume at these higher frequencies.

Although the spectral structure in figure 4 is qualitatively similar to that of the sound from the cylindrical bubble column in the experiment of Yoon *et al.* (1991) and Nicholas *et al.* (1994), there is one notable difference: the peaks in figure 4 are non-uniformly spaced, whereas the longitudinal resonances of the cylindrical bubble column are uniformly distributed in frequency (see, for example, fig. 4 in Nicholas *et al.* (1994), where the inter-peak spacing is *ca.* 71 Hz). The frequency differences between the peaks in figure 4 are 177 (first and second), 119 (second and third) and 113 Hz (third and fourth). This asymptotic approach to a uniform inter-peak spacing with increasing mode number is an important spectral feature of the sound from the bubble plume. Such behaviour is reminiscent of the zeros of the Bessel functions of the first kind, a point to which we shall return later.

Figure 5 shows a comparison between acoustic spectra from bubble plumes in the tank and in Lake Miramar. The tank spectrum shows slightly sharper peaks, due to the more stable environment in the laboratory, but the eigenfrequencies in the two spectra are almost identical. From this and other evidence, including the dependence of the eigenfrequencies on the properties of the jet (length, velocity and air entrainment ratio), reverberation in the tank is not considered to be responsible

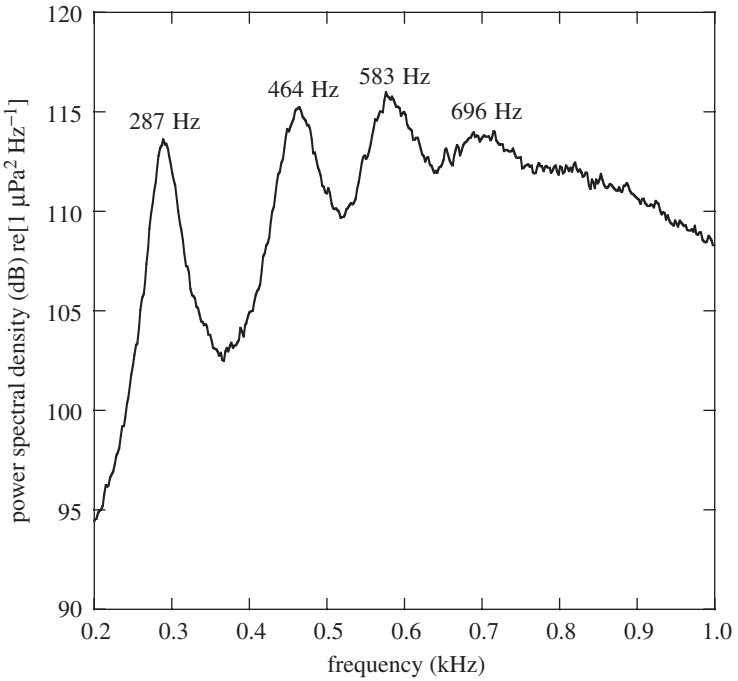

Figure 4. Spectrum of the acoustic signature of the bubble plume for jet velocity $u_j = 9.5\ \mathrm{m\,s^{-1}}$ and air entrainment ratio $q = 0.6$. The hydrophone was on the axis of the plume, 5 cm below the mean penetration depth. The noise floor in the tank in the absence of the jet was *ca.* 70 dB, at least 20 dB below the data.

for the spectral peaks in the laboratory data. Furthermore, the resonances of the tank had a negligible, if any, effect on the observed eigenfrequencies of the bubble plume. In the light of these conclusions, only tank data are discussed hereafter.

4. Scaling of the eigenfrequencies

Figure 6 shows a family of measured spectra for a range of values of the air entrainment ratio, q, with the jet velocity held constant at $u_j = 9.5\ \mathrm{m\,s^{-1}}$. As q is reduced, the frequency of each spectral peak shifts to a higher value. This effect is more clearly evident in figure 7, where, for a fixed $u_j = 9.5\ \mathrm{m\,s^{-1}}$, the first five eigenfrequencies are plotted as a function of q. By comparison with the slope of the reference line, it can be seen that each of the measured eigenfrequencies exhibits an inverse-fractional power-law scaling of the form $q^{-1/4}$.

The eigenfrequencies of the plume depend also on the jet velocity. Figure 8 shows the first five eigenfrequencies plotted against u_j for a fixed air entrainment ratio $q = 0.55$. In this case, as can be seen from the slope of the reference line, the eigenfrequencies vary accurately as $u_j^{-1/2}$. As shown later, this inverse square-root scaling is consistent with a sound-speed profile that varies as $x^{1/2}$, where x is the distance down the axis of the plume, as measured from the entry point of the jet.

By combining the dependencies exhibited in figures 7 and 8, the observed scaling of the eigenfrequencies of the bubble plume may be expressed as

$$f_m \propto u_j^{-1/2} q^{-1/4}, \tag{4.1}$$

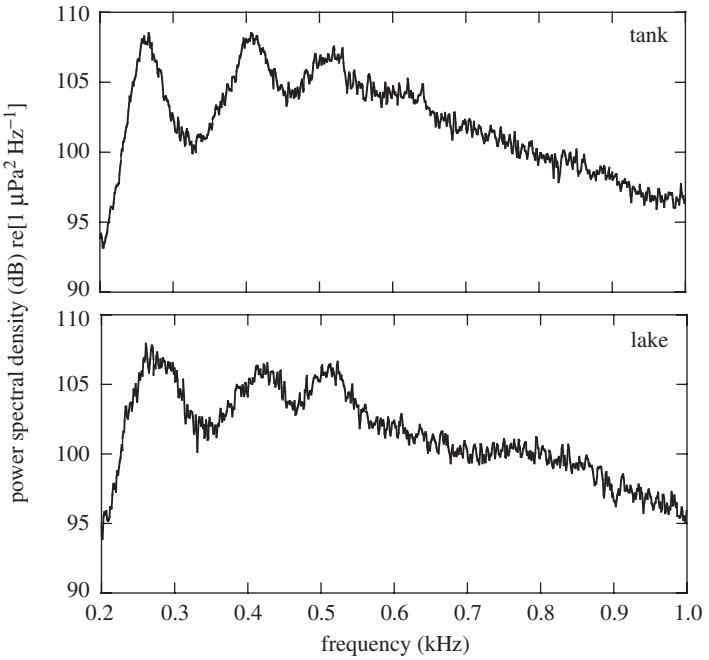

Figure 5. Comparison between sound-pressure spectra obtained in the tank and in Lake Miramar. In both cases shown, no entrainment nozzle was used, the jet velocity was $u_j = 9.5\ \mathrm{m\ s^{-1}}$ and the jet length was approximately 15 times the jet diameter. Under these conditions, the air entrainment ratio was $q \approx 0.9$.

where f_m is the frequency of the mth longitudinal mode of oscillation of the plume. The unspecified constant of proportionality in (4.1) shows a nonlinear dependence on m. At jet velocities below *ca.* $4\ \mathrm{m\ s^{-1}}$, the entrainment of air can be very irregular (van de Sande & Smith 1973), in which case the scalings in (4.1) may not hold, but, for the range of jet velocities and air entrainment ratios shown in figures 7 and 8, the proportionality in (4.1) is valid.

5. Geometry of the bubble plume

Gas entrainment by fluid flow is a complex dynamical phenomenon. Even for the simple case of a vertical plunging jet, the gas flux is a complicated function of viscosity and the parameters of the jet (velocity, length and diameter). Our acoustic experiments involved low-viscosity low-velocity entrainment in which small instabilities on the cylindrical surface of the jet make contact with the walls of an inverted meniscus, formed by Bernoulli suction, on the surface of the receiving pool (Bin 1988). As illustrated schematically in figure 9, when the jet velocity is greater than the entrainment threshold velocity, as in our case, air cavities are created as the instabilities collide with the meniscus and a plume of bubbles is formed beneath the entry point. The bubbles are transported downwards and laterally into the host fluid by turbulent diffusion, while buoyancy opposes the downward motion and eventually returns the entrained air to the surface. The net effect of these transport mechanisms is to create a bubble plume, which, on average, is axially symmetric and shaped like a cone with the apex at, or very close to, the water surface.

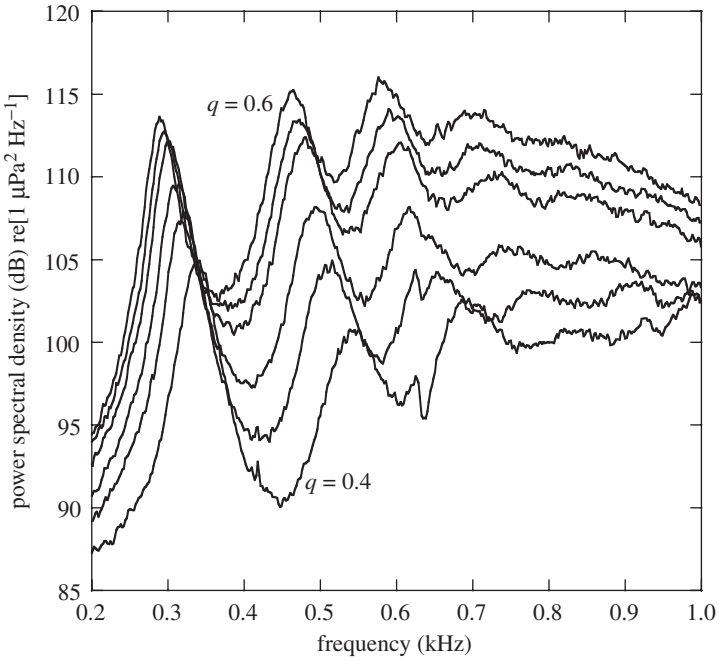

Figure 6. Family of sound-pressure spectra from the bubble plume with a constant jet velocity $u_j = 9.5\ \mathrm{m\ s^{-1}}$ and the air entrainment ratio taking the following values: $q = 0.40$, 0.45, 0.49, 0.53, 0.56 and 0.60.

The tank in which our acoustic experiments were performed has a viewing window in one side (figure 1), through which the bubble plume was photographed. Figure 10 shows a sequence of four instantaneous realizations, or 'snapshots', of the bubble plume, which illustrate the variability in the shape of the aerated region, a phenomenon related to intermittency (Hinze 1975; Townsend 1976). An average of 100 instantaneous realizations of the plume, taken over a period of 3 s, is shown in figure 11*a*. The averaging smoothes the variations in the geometry, thereby revealing the axially symmetric cone-like shape of the plume and its sharply delineated base. The remainder of the discussion is set entirely in the context of the geometrically well-defined average bubble plume, since the eigenfrequencies observed in the acoustic pressure spectrum themselves represent averages recorded over extended periods of time.

Although they appear sharp in figure 11*a*, the flanks of the biphasic conical plume are not abrupt lateral boundaries. Since the bubbles act as passive tracers, the lateral concentration of gas, or void fraction, follows the mean downward velocity profile of the turbulence, which decays smoothly with increasing horizontal distance from the axis of the plume. According to McKeogh & Ervine (1981), the mean downward velocity normal to the axis is well represented by a Gaussian distribution,

$$U(x,y) = U_x \exp\left(-\frac{1}{2}\frac{y^2}{x^2\tan^2\theta_2}\right), \tag{5.1}$$

where $y = x\tan\theta$ is the horizontal distance from the axis and U_x is the mean downward velocity of the turbulence on the axis at depth x below the apex. (The

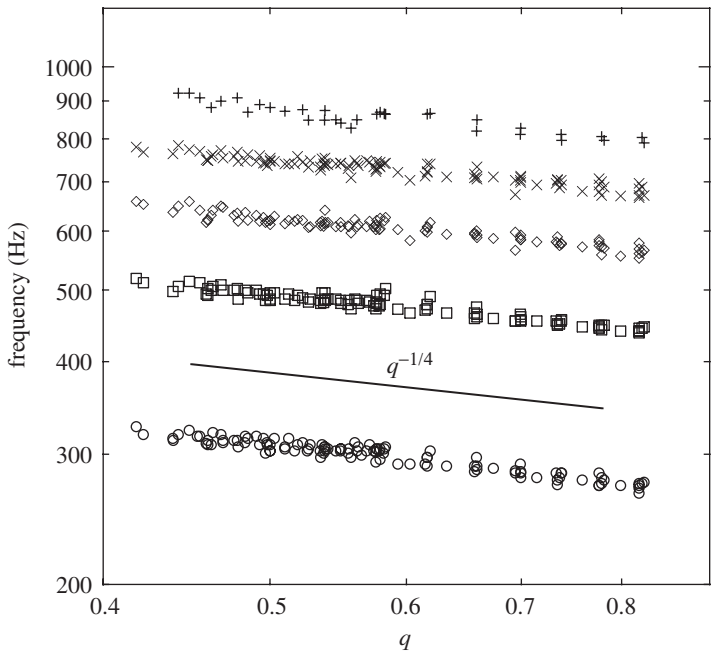

Figure 7. The first five eigenfrequencies as a function of the air entrainment ratio, q, for a fixed jet velocity of $u_\mathrm{j} = 9.5$ m s^{-1}. (Note that both axes are logarithmic.) Key: ○, mode 1; □, mode 2; ◇, mode 3; ×, mode 4; +, mode 5. The solid reference line indicates an inverse fourth-root scaling, that is, frequency $\propto q^{-1/4}$.

Cartesian and polar coordinate systems used in discussing the plume are illustrated in figure 11*b*.) The half-angle of the cone, θ_2, as defined by (5.1), occurs where the mean downward turbulent velocity has decayed to $1/\sqrt{\mathrm{e}}$ of the centre-line value; and the subscript 2 on the half-angle denotes 'two phase'.

In the absence of air entrainment, an identical expression to (5.1) describes the mean downward turbulent velocity (Tennekes & Lumley 1972) except that, in the single-phase case, the half-angle of the cone, θ_1, is less than θ_2 by a factor of *ca.* 2. Evidently, the introduction of air increases the turbulence below the entry point, which broadens the cone angle. As a canonical model of fluid mechanics and turbulence theory, the single-phase turbulent plume has been studied extensively (Hinze 1975; Tennekes & Lumley 1972; Townsend 1976; Wygnanski & Fiedler 1969) and it is well established that the half-angle is $\theta_1 \approx 4^\circ$.

Comparatively little is known about the mean turbulent velocity distribution in the plume of the biphasic jet. As reported by Bin (1993), van de Donk (1981) has made direct measurements of the void fraction, β, in the bubbly plume, which, because the bubbles act essentially as passive tracers locked to the turbulent flow, is expected to show the same lateral decay as the mean downward advection-velocity distribution. Thus the dependence of β on horizontal distance from the axis is taken to show the same Gaussian form as the mean velocity,

$$\beta(x, y) = \beta_x \exp\left(-\frac{1}{2}\frac{y^2}{x^2 \tan^2 \theta_2}\right), \tag{5.2}$$

where β_x is the void fraction on the axis at depth x below the apex.

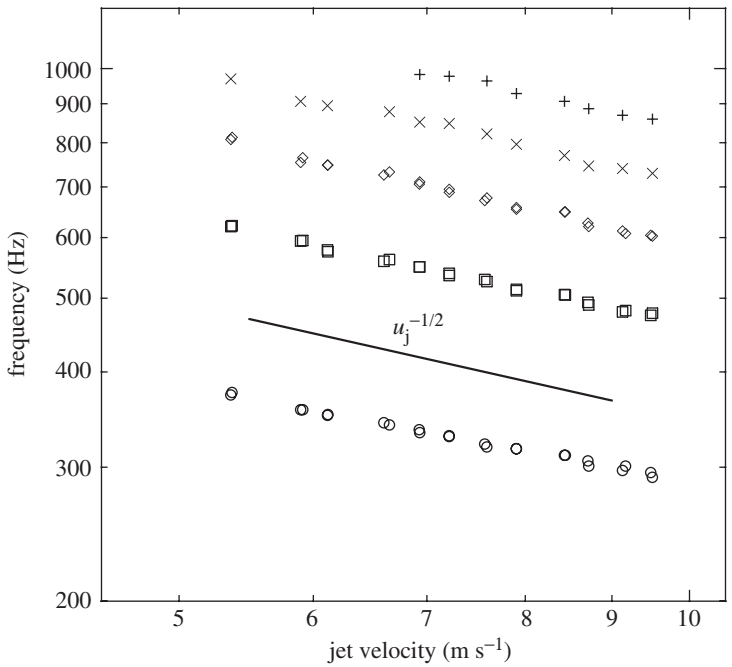

Figure 8. The first five eigenfrequencies as a function of the jet velocity, u_j, for a fixed air entrainment ratio, $q = 0.55$. (Note that both axes are logarithmic.) Key: ○, mode 1; □, mode 2; ◇, mode 3; ×, mode 4; +, mode 5. The solid reference line indicates an inverse square-root scaling, that is, frequency $\propto u_j^{-1/2}$.

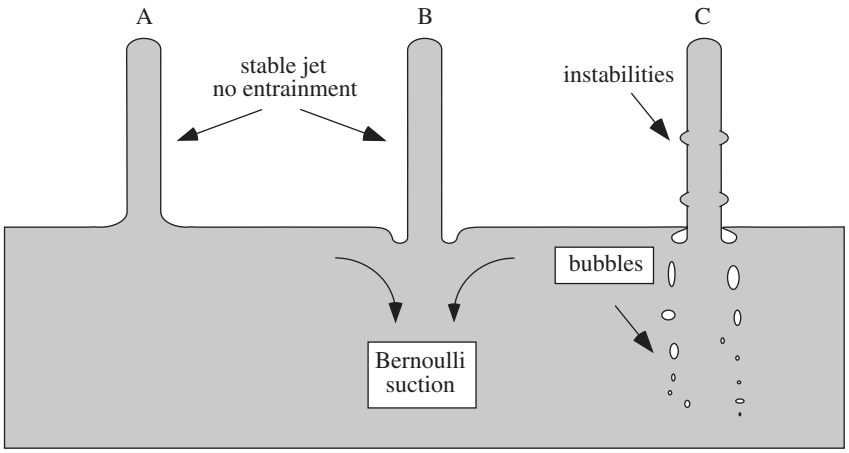

Figure 9. Schematic of bubble formation as a vertical jet penetrates an air-to-water interface. At A, the jet velocity is too low to invert the meniscus. At B, Bernoulli suction creates the meniscus, but the jet velocity is too low for air entrainment. At C, instabilities on the jet lead to air entrainment and the creation of bubbles.

Van de Donk's (1981) void-fraction data are shown in fig. 31 of Bin (1993), and it is readily confirmed that (5.2) fits these data remarkably well. For the half-angle, the data taken midway along the flanks of the bubble plume yield directly $\theta_2 \approx 7.5°$.

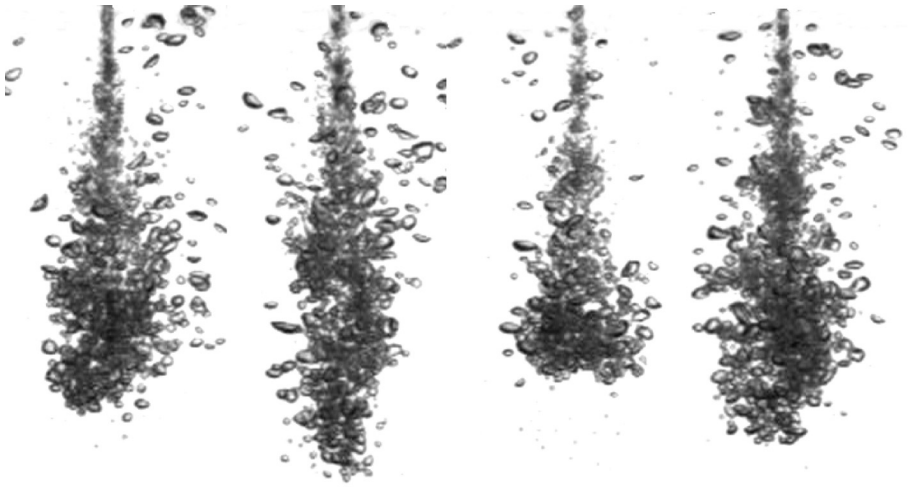

Figure 10. Four instantaneous realizations of the cone-like plume of bubbles formed by a vertical plunging freshwater jet. In all four cases, the radius of the jet was $R_j = 0.8$ mm and the jet velocity was $u_j = 6\ \mathrm{m\ s^{-1}}$. The length of the plumes is of the order of 12 cm.

This is consistent with McKeogh & Ervine's (1981) expressions for the mean velocity on the axis of the cone in which the constant for the biphasic flow is approximately twice that for the single-phase case. (This constant scales directly with the tangent of the cone angle.)

The base of the bubble plume, which, unlike the flanks, is sharply delineated, occurs at a depth r_p on the axis, where r_p is generally referred to as the penetration depth (figure 11*b*). This is the depth at which the downward flow of the bubbles due to turbulent advection is balanced by buoyancy. At the penetration depth, the mean downward velocity is equal to the terminal speed, U_T, of the bubbles. In fresh water, the bubbles at the base of the plume are *ca.* 4 mm in diameter, independent of the experimental parameters (Berger 1999; Bin 1976; Evans 1990; Evans *et al.* 1992; Smigelschi & Suciu 1976). For bubbles around this size, the terminal speed is insensitive to the diameter (Maxworthy *et al.* 1996), with a value $U_T \approx 0.24\ \mathrm{m\ s^{-1}}$. The cap-like shape of the bubble plume between the conical region above and the penetration depth below is determined by the terminal speed of the bubbles (Berger 1999): the curve of the cap is the locus of the points where the mean advection velocity equals U_T.

Part II. Theory

6. Dynamics of the flow

It is evident from the pressure spectra in figures 4–8 that the bubble plume acts as a leaky resonant cavity, creating a sound-pressure field in the surrounding water. Since the resonance frequencies of the individual bubbles in the plume are significantly higher than the observed eigenfrequencies, it may be inferred that the aerated region acts as a continuum in which the bubbles undergo coherent collective oscillations. The peaks observed in the near-field pressure spectrum occur at the eigenfrequencies of the bubbly cavity. These eigenfrequencies are determined by two factors, the

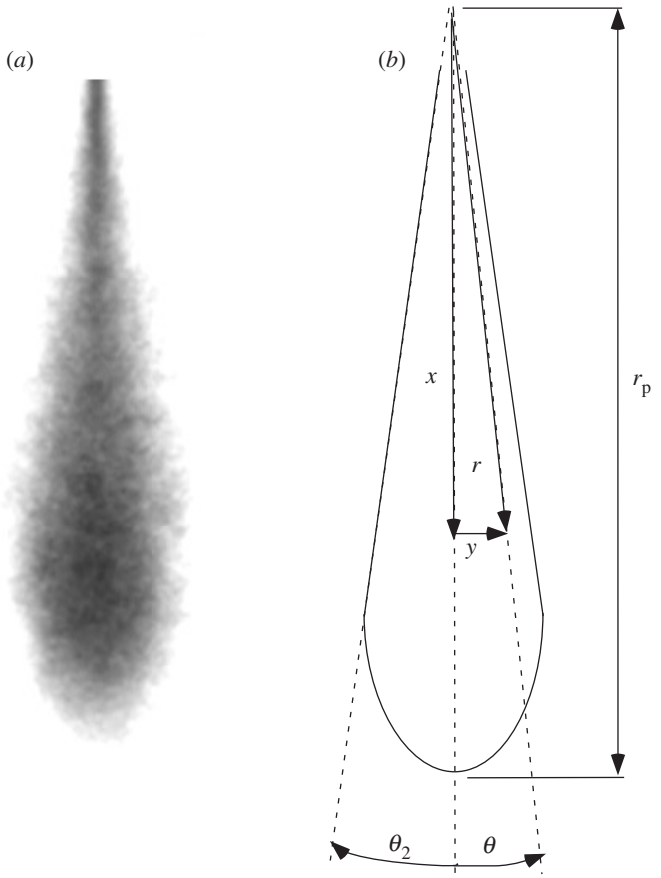

Figure 11. (*a*) Average of 100 instantaneous bubble plumes taken over a period of *ca.* 3 s. (*b*) Geometry of the conical bubble plume, the penetration depth and Cartesian and polar coordinate systems.

geometry of the plume and the sound-speed distribution within the plume. The latter is not expected to be uniform, since it depends on the void fraction, which itself varies within the cavity. An analogous void-fraction distribution has been observed in bubble clouds under breaking waves by Lamarre & Melville (1994).

The void fraction as a function of position in the plume is given in (5.2), but incompletely because the vertical profile, β_x, is as yet unspecified. To determine β_x, two conditions are invoked, the conservation of mean downward momentum flux and the conservation of gas-volume flux through the plume, both of which involve integrals over the horizontal radius, y, of the form

$$I_n = \int_0^\infty y \exp\left(-\frac{ny^2}{2x^2 \tan^2\theta_2}\right) \mathrm{d}y = \frac{x^2 \tan^2\theta_2}{n}, \quad n = 1, 2, 3. \tag{6.1}$$

Momentum-flux conservation requires that

$$u_\mathrm{j}^2 \rho_\mathrm{w} \pi R_\mathrm{j}^2 = 2\pi U_x^2 \rho_\mathrm{w} (I_2 - \beta_x I_3), \tag{6.2}$$

where R_j is the radius of the jet and ρ_w is the density of water. The term on the left-hand side of (6.2) is the momentum flux in the jet and that on the right-hand

side is the mean downward momentum flux through the horizontal plane at depth x below the entry point of the jet. For the air-volume flux, Q_{a}, to be conserved, we must have

$$Q_{\mathrm{a}} = 2\pi\beta_x U_x I_2, \tag{6.3}$$

or, alternatively in terms of the air entrainment ratio q,

$$q = \frac{Q_{\mathrm{a}}}{Q_{\mathrm{w}}} = \frac{2\beta_x U_x I_2}{u_{\mathrm{j}} R_{\mathrm{j}}^2}, \tag{6.4}$$

where $Q_{\mathrm{w}} = \pi u_{\mathrm{j}} R_{\mathrm{j}}^2$ is the water-volume flux in the jet. Equations (6.3) and (6.4) can be solved for β_x and U_x, yielding

$$\beta_x = \frac{2q^2 r_1^2}{3x^2}\left[\sqrt{1+\frac{9x^2}{4q^2 r_1^2}} - 1\right] \approx q\frac{r_1}{x} \tag{6.5}$$

and

$$U_x = \frac{3u_{\mathrm{j}}}{2q}\left[\sqrt{1+\frac{9x^2}{4q^2 r_1^2}} - 1\right]^{-1} \approx u_{\mathrm{j}}\frac{r_1}{x}, \tag{6.6}$$

where

$$r_1 = \frac{R_{\mathrm{j}}}{\tan\theta_2}. \tag{6.7}$$

The approximations in (6.5) and (6.6) are valid provided $x \gg r_1 \approx 6\,\mathrm{mm}$, where the numerical value is representative of the bubble plumes in our experiments.

The on-axis penetration depth, $x = r_{\mathrm{p}}$, is immediately available from (6.6) by setting U_x equal to the terminal velocity, U_{T}. This yields

$$r_{\mathrm{p}} = r_1\frac{u_{\mathrm{j}}}{U_{\mathrm{T}}}\sqrt{1+\frac{4}{3}\frac{qU_{\mathrm{T}}}{u_{\mathrm{j}}}} \tag{6.8a}$$

$$\approx r_1\frac{u_{\mathrm{j}}}{U_{\mathrm{T}}}, \tag{6.8b}$$

where the approximation states that the penetration depth scales inversely as the terminal velocity and in direct proportion to the jet velocity, both of which are consistent with the observations of Clanet & Lasheras (1997) on the biphasic jet. For the jet velocities used in our experiments, ranging between 4 and $10\,\mathrm{m\,s^{-1}}$, r_{p} takes values between 10 and 24 cm, and thus the approximations in (6.5), (6.6) and (6.8*b*) are valid everywhere in the plume except immediately beneath the entry point of the jet. Since this region has little, if any, effect on the low-frequency sound-pressure field, the approximate forms for β_x and r_{p} are used exclusively in the acoustic analysis developed later in § 9.

According to the approximation in (6.5), the void fraction down the axis of the plume decays inversely with depth. When this result is substituted into (5.2), the void fraction throughout the plume can be written as

$$\beta(r,\theta) \approx q\left(\frac{r_1}{r}\right)f(\theta), \tag{6.9}$$

where

$$f(\theta) = (\cos\theta)^{-1} \exp\left(-\frac{1}{2}\frac{\tan^2\theta}{\tan^2\theta_2}\right). \tag{6.10}$$

In these expressions, the Cartesian coordinates (x, y) have been converted to spherical coordinates (r, θ), with the origin at the apex of the cone (figure 11*b*): r is distance from the apex to the point (x, y) and θ is the polar angle, that is, the angular distance from the axis to the point (x, y). Similarly, from (5.1) and (6.6), the mean downward velocity distribution is

$$U(r, \theta) \approx u_{\mathrm{j}}\left(\frac{r_1}{r}\right) f(\theta), \tag{6.11}$$

which is included for completeness but will not be referred to again.

7. Sound-speed distribution in the plume

For the acoustic analysis developed in § 9, the sound-speed distribution in the plume is required. Assuming, for the moment, that the resonance frequencies of individual bubbles are well above the eigenfrequencies of the plume, the bubbly medium may be treated as a two-phase continuum, in which case the sound speed, $c(r, \theta)$, is related to the void fraction, $\beta(r, \theta)$, through Wood's equation (Wood 1964),

$$c = \frac{1}{\sqrt{K\rho}}, \tag{7.1}$$

where $\rho \equiv \rho(r, \theta)$ and $K \equiv K(r, \theta)$ are, respectively, the density and compressibility of the biphasic medium. These variables are simple weighted means in which the weighting coefficients depend linearly on β,

$$\rho = \beta\rho_{\mathrm{a}} + (1 - \beta)\rho_{\mathrm{w}} \tag{7.2}$$

and

$$K = \beta K_{\mathrm{a}} + (1 - \beta)K_{\mathrm{w}}, \tag{7.3}$$

where the subscripts 'a' and 'w' denote air and water, respectively. By substituting for K and ρ in (7.1), the expression for the sound speed becomes

$$c = \{[\beta\rho_{\mathrm{a}} + (1 - \beta)\rho_{\mathrm{w}}][\beta K_{\mathrm{a}} + (1 - \beta)K_{\mathrm{w}}]\}^{-1/2}, \tag{7.4}$$

which is the classic form of Wood's equation for the sound speed in a two-phase medium. As reported by Carey & Browning (1988), Wood's equation has been verified experimentally by Karplus (1958) for void fractions up to 80%.

In § 8 below, it is shown that, for low frequencies, below the breathing mode frequency of individual bubbles in the plume, equation (7.4) should be valid for the sound-speed distribution in the conical cavity beneath the jet. Figure 12 shows (7.4) plotted over six decades of void fraction, from 10^{-6} to 1. For intermediate void fractions, between 10^{-4} and 10^{-1}, the expression for the sound speed in (7.4) reduces to the approximate form

$$c \approx \frac{1}{\sqrt{\beta\rho_{\mathrm{w}}K_{\mathrm{a}}}} = \sqrt{\frac{\gamma P_0}{\beta\rho_{\mathrm{w}}}}, \tag{7.5}$$

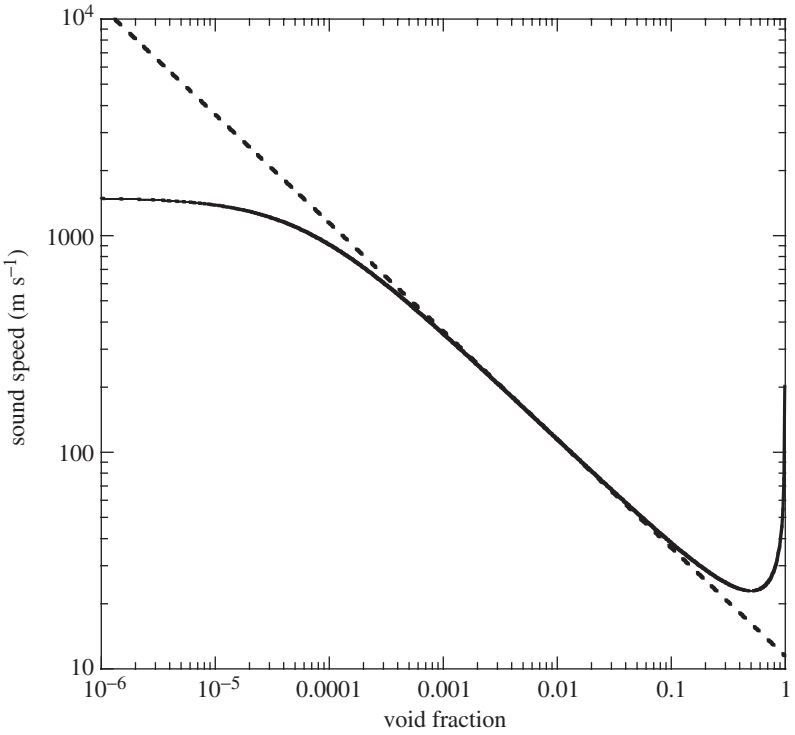

Figure 12. Sound speed computed as a function of void fraction from Wood's equation (7.4) (solid line), and the approximation in (7.5) (dashed line). Table 1 shows the parameter values used in evaluating the expressions.

indicating that, in this regime, the sound speed scales inversely as the square root of the void fraction. In the second radical in (7.5), the compressibility, K_{a}, has been equated to $(\gamma P_0)^{-1}$, where $P_0 = 101.3\,\mathrm{kPa}$ is the ambient pressure and γ is the polytropic index of the air in the bubbles constituting the plume. According to Leighton (1994), $\gamma \approx 1.3$ is an appropriate value for a bubble with radius of order 1 mm—as found throughout much of the plume—at a frequency in the region of 500 Hz. A plot of (7.5) is included in figure 12 to illustrate the range over which the approximation is valid.

The void fractions within the bubble plume are well within the range where (7.5) satisfactorily approximates Wood's equation (see figure 16*a*). By combining (6.8) and (7.5), the sound speed is seen to scale as the square root of the radial distance, r, from the apex down into the plume,

$$c \approx \alpha \sqrt{\frac{r}{f(\theta)}}, \tag{7.6}$$

where

$$\alpha = \sqrt{\frac{\gamma P_0}{q r_1 \rho_{\mathrm{w}}}}. \tag{7.7}$$

Note that α depends on the air entrainment ratio, q, the jet radius, R_{j}, and the cone angle, θ_2, but is independent of the jet velocity, u_{j}. Obviously, down the axis of the

plume, where $f(0) = 1$, we may replace r by x in (7.6) to obtain $c_x \approx \alpha\sqrt{x}$. At this point, it may be anticipated that the square-root sound-speed profile in (7.6) will play an important role in characterizing the spectral properties of the acoustic field in the water surrounding the plume.

8. Effect of bubble size

Before proceeding with the acoustic argument, it is as well to examine the validity of (7.5) in the context of the bubble plume, since this approximate form of Wood's equation plays a crucial role in the analysis of the longitudinal resonances of the conical biphasic domain. Equation (7.5) is a low-frequency approximation, which should hold provided the resonance frequencies of the individual bubbles in the plume are not too close to the eigenfrequencies of the bubbly cavity. To investigate whether this rather loose condition is satisfied, the bubble-size distribution is needed. Unfortunately, little is known about the bubble sizes except that the upper part of the plume is populated by the smallest, or primary, bubbles and the lower part by larger secondary bubbles. Several experimental observations (Berger 1999; van de Sande 1974; van de Sande & Smith 1975) indicate that the primary bubbles in fresh water are less than 1 mm in radius and also that no short-lived larger bubbles are present. According to Minnaert (1933), the radial-mode resonance angular frequency, ω_0, of a bubble of radius a is

$$\omega_0 = \frac{1}{a}\sqrt{\frac{3\gamma P_0}{\rho_{\mathrm{w}}}}, \tag{8.1}$$

where, as before, P_0 is the equilibrium pressure and γ is the polytropic index of the gas in the bubble. From (8.1), a bubble of 1 mm radius has a resonance frequency of *ca.* 3.3 kHz, which is well above the eigenfrequencies of the bubble-plume cavity. Thus, as far as the small primary bubbles are concerned, equation (7.5) is a satisfactory approximation. The situation is not quite so clear for the secondary bubbles in the lower part of the plume, which have a radius of 2 mm, corresponding to a monopole resonance frequency of 1.6 kHz. This is a factor of only 2 to 3 above the eigenfrequencies of the plume.

To determine whether (7.5) is valid in the presence of the secondary bubbles, we follow Hahn (1999) in considering the classic expression for the sound speed of a low-void-fraction bubbly fluid at or near the monopole resonance frequency, $\omega_0/2\pi$, of the bubbles (Carstensen & Foldy 1947; Feuillade 1996; Foldy 1945),

$$c = \left(K_{\mathrm{w}}\rho_{\mathrm{w}} + \frac{3\beta/a^2}{\omega_0^2 - \omega^2}\right)^{-1/2}, \tag{8.2}$$

where losses have been neglected. By substituting Minnaert's expression in (8.1) for ω_0 and neglecting the term in K_{w}, the compressibility of the fluid, equation (8.2) reduces to the low-frequency form

$$c \approx \sqrt{\frac{\gamma P_0}{\rho_{\mathrm{w}}\beta}} \quad \text{for } \omega \ll \omega_0, \tag{8.3}$$

which is identical to the approximation for Wood's equation in (7.5). Equations (8.2) and (8.3) may be compared in figure 13, where they are plotted as a function of

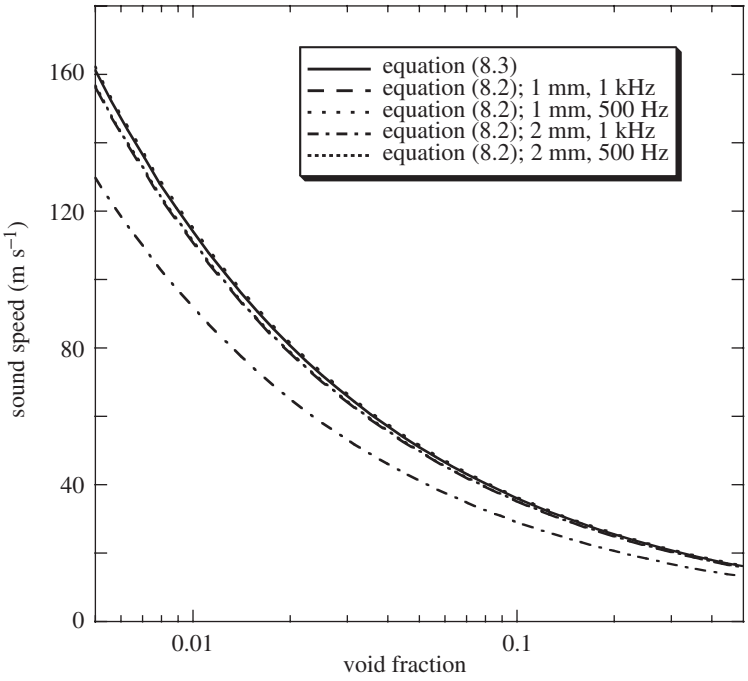

Figure 13. Sound speed computed as a function of void fraction, taking account of bubble size. As shown in the inset, the various broken lines are from Foldy's expression in (8.2) for different combinations of bubble radius and frequency. The solid line is the approximation for Wood's equation in (7.5) and (8.3).

the void fraction. It can be seen that, even with the extreme combination of *large* bubbles of radius 2 mm in a *small* bubble cloud of resonance frequency 1 kHz, the low-frequency approximation to Wood's equation is not too unreasonable. At more representative combinations of cloud frequency and bubble size, the approximation is almost indistinguishable from the full expression in (8.2), signifying that bubble-size effects, even for the large secondary bubbles, are negligible at the longitudinal resonance frequencies of our bubble plumes. Accordingly, equation (7.5) may be used with confidence to relate the sound speed to the void fraction throughout the bubbly medium.

9. Acoustic field in the bubble-plume cavity

Since acoustic transmission from the leaky bubble plume is a linear process, the spectral peaks in the sound-pressure field external to the plume will occur at the same frequencies as those in the spectrum of the internal field. To determine these eigenfrequencies, it is therefore necessary to consider only the field within the bubble-plume cavity. The Green function is the solution of the Helmholtz equation

$$\nabla^2\psi + \frac{\omega^2}{c^2}\psi = -s\delta(\boldsymbol{r} - \boldsymbol{r}'), \tag{9.1}$$

where ∇^2 is the Laplacian, ω is angular frequency, s is the frequency-dependent source strength, δ is the Dirac delta function and $\psi(\boldsymbol{r}, \boldsymbol{r}')$ is the velocity potential at position $\boldsymbol{r}$ due to a point source at $\boldsymbol{r}'$.

Given the conical symmetry of the plume, illustrated in figure 11, the spherical polar coordinate system with the origin at the apex is the natural choice for the problem. On average, the acoustic field from the plume is azimuthally uniform, implying an axisymmetric source distribution. Taking the simplest case, a point source on the axis, the Helmholtz equation becomes

$$\frac{1}{r^2}\frac{\partial}{\partial r}\left(r^2\frac{\partial \psi}{\partial r}\right) + \frac{1}{r^2\sin\theta}\frac{\partial}{\partial \theta}\left(\sin\theta\frac{\partial \psi}{\partial \theta}\right) + \frac{\omega^2}{\alpha^2 r}f(\theta)\psi = -s\frac{\delta(r-r')\delta(\theta)}{r^2\sin\theta}, \qquad (9.2)$$

where $(r', 0)$ and (r, θ) are the source and receiver coordinates, respectively, and the expression in (7.6) for the sound-speed distribution within the plume has been used. Acoustic attenuation in the bubble plume has been neglected in (9.2), since dissipation will not shift the resonance peaks appreciably.

The boundary conditions to be satisfied by the field are now considered. Since the free surface of the pool is a pressure-release boundary for sound incident from below, we must have $\psi = 0$ for $\theta = \frac{1}{2}\pi$. At the base of the plume, the penetration depth represents a sharp demarcation between the two-phase bubbly region above and the single-phase fluid below. This boundary is approximated as an acoustically rigid base cap. An intuitive justification for the rigid condition is as follows. From (7.6), the sound speed in the bubbly region at the penetration depth is less than $100\,\mathrm{m\,s^{-1}}$ (see figure 16*b*), which is at least an order of magnitude less than the sound speed in the single-phase turbulent water immediately beneath the plume. For the low-order modes associated with the low-frequency spectral peaks, a plane-wave decomposition would lead to equivalent rays that are at near-normal incidence to the bottom boundary. When these two conditions hold, that is, near-normal incidence and a large external-to-internal sound-speed ratio, the Rayleigh reflection coefficient is $V \approx 1$, indicating that the small, almost planar, element of the boundary intersected by an equivalent ray is essentially rigid. A similar situation is encountered in a sphere of sound speed c_1 embedded in a medium of sound speed $c_2 > c_1$. In this case, with a point source at the centre, a wave-theoretic analysis shows formally that the internal curved boundary of the sphere becomes rigid in the limit as c_2/c_1 goes to infinity.

Figure 14*a* illustrates the pressure-release under-surface of the pool and the acoustically hard lower boundary of the bubble plume; but even with these boundaries specified, the problem is still intractable. The main difficulty is that the Helmholtz equation is not separable, in part due to the angular dependence of the sound speed represented by the function $f(\theta)$ in the last term on the left-hand side of (9.2). To take account of $f(\theta)$, we introduce a 'small-angle approximation', bearing in mind that the angular width of the bubbly cavity is quite narrow, with $\theta_2 \approx 7.5°$. For the purpose of determining the acoustic field within this small angular region, we firstly neglect the angular variation in the sound speed by setting $f(\theta)$ to unity, secondly we introduce a fictitious pressure-release conical boundary with half-angle $\theta_f > \theta_2$, and finally the new conical domain is closed with a rigid spherical base, centred on the apex, as shown in the schematic of figure 14*b*. Under these conditions, the Helmholtz equation is separable, that is, its solution may be expressed as the product of a function of range and a function of angle. It should be emphasized that this solution is valid only for small angles, close to the axis of the plume. The half-angle,

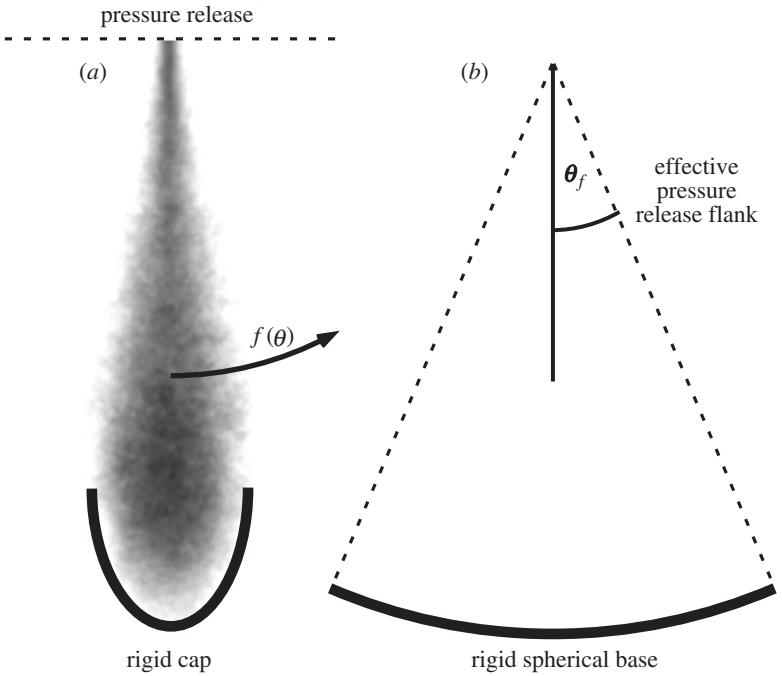

Figure 14. (*a*) Boundary conditions and angle-dependent sound speed, $f(\theta)$, in the actual bubble plume. (*b*) Effective conical domain with pressure-release flanks, rigid spherical base centred on the apex and angle-independent sound speed used in the small-angle approximation for the acoustic field in the bubble-plume cavity.

θ_f, of the effective cone is an unknown parameter, which is to be determined from a comparison of the predicted eigenfrequencies with the measured values.

By adjusting the position of the pressure-release flanks, we are able to control the angular dependence of the acoustic field close to the axis of the plume. A small value of θ_f yields strong curvature in the field and vice versa. The effect of the angular variation of the sound speed, $f(\theta)$, in the actual plume is replicated in the effective cone by the judicious placement of its pressure-release flanks. The concept of an effective pressure-release boundary was introduced, in a slightly different context, by Weston (1960) and applied by Buckingham to the analysis of acoustic propagation in shallow-water channels (Buckingham 1979) and penetrable wedges (Buckingham 1987).

Returning to (9.2), it is convenient to introduce a new field variable, w, where

$$\psi = \frac{w}{\sqrt{r}} \tag{9.3}$$

and to make the coordinate transformation

$$z = 2\frac{\omega}{\alpha}\sqrt{r}. \tag{9.4}$$

The Helmholtz equation then becomes

$$\frac{\partial^2 w}{\partial z^2} + \frac{1}{z}\frac{\partial w}{\partial z} - \frac{w}{z^2} + \frac{4}{z^2 \sin\theta}\frac{\partial}{\partial \theta}\left(\sin\theta \frac{\partial w}{\partial \theta}\right) + w = -s\frac{8\omega}{\alpha}\frac{\delta(z^2 - z'^2)\delta(\theta)}{z\sin\theta}, \tag{9.5}$$

where

$$z' = 2\frac{\omega}{\alpha}\sqrt{r'} \tag{9.6}$$

and, in the spirit of the small-angle approximation, $f(\theta)$ has been set to unity. As shown in the appendix, equation (9.5) can be solved, subject to the boundary conditions illustrated in figure 14*b*, by the application of a Legendre transform over polar angle, θ, and a finite Hankel transform over radial depth, r. Although the full solution containing all the angular modes, that is, for $i = 1, 2, \ldots$, appears in (A 19), it may be anticipated that only the lowest-order angular mode, for which $i = 1$, is required for the low-frequency resonances of the bubble plume. The higher-order angular modes also yield spectral peaks, but at frequencies well above those observed in the experiments.

The first term in the modal expansion of (A 19) is

$$w(z,\theta) = -\frac{2\pi s}{z'}\frac{\omega}{\alpha}A_\nu \frac{J_{\mu_i}(z')}{[z_\mathrm{p}J'_{\mu_i}(z_\mathrm{p}) - J_{\mu_i}(z_\mathrm{p})]}F(z,z_\mathrm{p})P_\nu(\cos\theta), \tag{9.7}$$

where $J_\mu(\cdot)$ is the Bessel function of the first kind of order μ, $P_\nu(\cos\theta)$ is the Legendre function of the first kind of degree ν and

$$z_\mathrm{p} = 2\frac{\omega}{\alpha}\sqrt{r_\mathrm{p}}. \tag{9.8}$$

The function F is

$$F(z,z_\mathrm{p}) = J_\mu(z)[Y_\mu(z_\mathrm{p}) - z_\mathrm{p}Y'_\mu(z_\mathrm{p})] + Y_\mu(z)[z_\mathrm{p}J'_\mu(z_\mathrm{p}) - J_\mu(z_\mathrm{p})], \tag{9.9}$$

where $Y_\mu(\cdot)$ is the Bessel function of the second kind of order μ. The primes on the Bessel functions in (9.7) and (9.9) denote differentiation with respect to the argument. For brevity in these expressions, we have set

$$\mu = [1 + 4\nu(\nu+1)]^{1/2} = (2\nu+1) \tag{9.10}$$

and the subscript $i = 1$ on ν, μ and F has been dropped, it being understood that hereafter these variables relate only to the first angular mode. Note that no Legendre function of the second kind appears in (9.7), since such functions diverge on the axis of the cone.

The degree, ν, of the Legendre function in (9.7) must be such as to satisfy the pressure-release boundary condition on the flanks of the effective cone,

$$P_\nu(\cos\theta_f) = 0. \tag{9.11}$$

This constraint indicates that ν and θ_f are not independent. In fact, ν, rather than θ_f, appears explicitly in the solution for the eigenfrequencies, and it is ν that is to be determined empirically by comparing the predicted eigenfrequencies with the data. The half-angle of the effective cone, although not needed, may then be computed from (9.11).

10. The eigenfrequencies

At the eigenfrequencies, the function in (9.7) exhibits poles, which represent a set of longitudinal resonances of the conical cavity. The poles occur at the zeros of the function in square brackets in the denominator of (9.7),

$$X_\mu(z_\mathrm{p}) = z_\mathrm{p}J'_\mu(z_\mathrm{p}) - J_\mu(z_\mathrm{p}), \tag{10.1}$$

which is a well-known function in the theory of Bessel functions (Lebedev 1965; Watson 1958). For our case, where $\mu = 1$, X_μ has an infinite number of real positive roots and no complex roots.

If the mth zero of X_μ is denoted by $z_{\mu,m}$, the eigenfrequency, $f_m = \omega_m/2\pi$, of the mth longitudinal mode is obtained from the condition

$$z_{\mu,m} = 2\frac{\omega_m}{\alpha}\sqrt{r_\mathrm{p}}, \tag{10.2}$$

where the right-hand side is just the value of z_p, from (9.8), at frequency f_m. It follows from (10.2) that the eigenfrequencies are

$$f_m = \frac{z_{\mu,m}}{4\pi}\frac{\alpha}{\sqrt{r_\mathrm{p}}}, \quad m = 1, 2, \ldots, \tag{10.3}$$

which, on substituting for the penetration depth, r_p, from (6.8) and for α from (7.7), becomes

$$f_m = \frac{\tan\theta_2}{4\pi R_\mathrm{j}}\sqrt{\frac{\gamma P_0 U_\mathrm{T}}{\rho_\mathrm{w}}}z_{\mu,m}q^{-1/2}u_\mathrm{j}^{1/2}. \tag{10.4}$$

Equation (10.4), the central result of our analysis, states that the eigenfrequencies of the longitudinal modes are non-uniformly spaced in the spectrum of the acoustic field, scaling in proportion to the zeros, $z_{\mu,m}$, of the function X_μ. Qualitatively, this non-uniform distribution of the spectral peaks is consistent with the data shown in figures 6–8. For a quantitative comparison with the data, the zeros of X_μ must be evaluated, which can only be done once μ has been determined. The theoretical scaling laws, however, may be discussed independently of the zeros.

The eigenfrequencies predicted by (10.4) are inversely proportional to the square root of the jet velocity, u_j, in excellent agreement with the slope of the data shown in figure 8. Had the sound-speed profile been taken as uniform throughout the plume, the eigenfrequencies would have been found (incorrectly) to scale inversely with the jet velocity, u_j^{-1}, rather than $u_\mathrm{j}^{-1/2}$. Evidently, the positions of the observed peaks in the sound-pressure spectrum are governed by the square-root scaling of the sound-speed profile, $c \propto \sqrt{r}$, in the bubble plume. The theoretical eigenfrequencies in (10.4) scale inversely with the square root of the air entrainment ratio, q. This scaling is a little steeper than that of the data in figure 7, which shows a slope closer to $q^{-1/4}$.

11. Empirical correction for the *q*-scaling

A factor that may account for the small discrepancy between the theoretical and observed q-scalings of the eigenfrequencies concerns the penetration depth, r_p, which has been observed to show a weak dependence on q (see figure 15*b*) of the form (Hahn 1999; van de Sande & Smith 1975)

$$r_\mathrm{p} \propto q^{-1/4}. \tag{11.1}$$

According to (6.8), r_p is inversely proportional to $\tan\theta_2$, suggesting that the q dependence of r_p could arise from a slight increase in the half-angle, θ_2, as more air is forced into the plume. Although no direct measurements of θ_2 as a function of q are available, the idea that more bubbles increase the lateral spreading of the turbulence is an extension of the observed fact that the half-angle of the biphasic plume is about

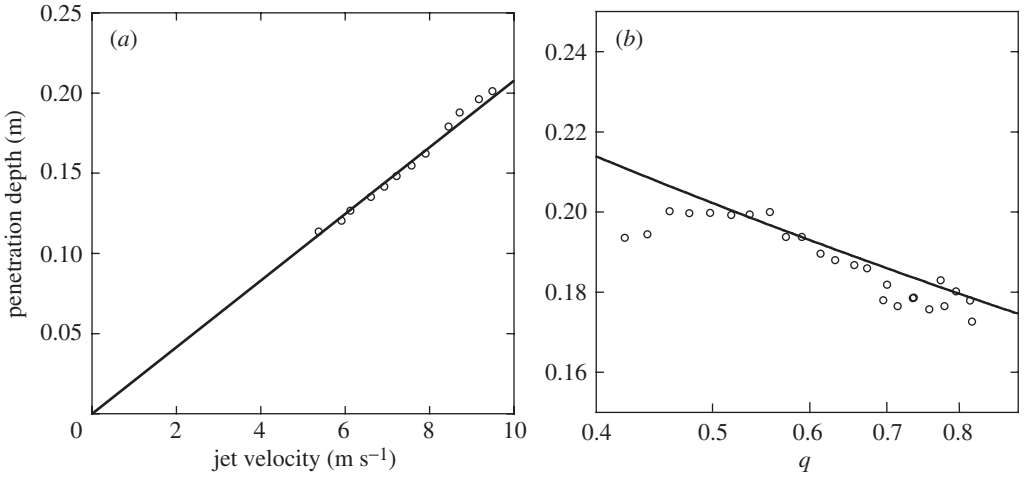

Figure 15. (*a*) Penetration depth as a function of jet velocity, u_j. The data (○) were taken with $q = 0.55$ and the solid line is the best fit of (11.3). (*b*) Penetration depth data (○) as a function of air entrainment ratio, q, with $u_\mathrm{j} = 9.5\ \mathrm{s}^{-1}$. The solid line is (11.3) evaluated using $q_0 = 0.25$.

twice that of the single-phase cone. A second mechanism, which could give rise to an *apparent* increase in the half-angle as q rises, is a reduction in r_p due to the drag of the bubbles on the turbulent flow. The phenomenon of bubble drag and its effects on the penetration depth of the plume in fresh and salt water have been investigated by Berger *et al.* (2003).

Whatever the underlying physics, equation (11.1) is consistent with a dependence of the form

$$\tan\theta_2 \propto q^{1/4}, \tag{11.2}$$

which leads to a scaling of $q^{-1/4}$ for the eigenfrequencies in (10.4), in very good agreement with the slope of the data in figure 7. To formalize the effects of the empirical relationship in (11.2), we replace $\tan\theta_2$ by $(q/q_0)^{1/4}\tan\theta_2$ in (6.8) for the penetration depth and in (10.4) for the eigenfrequencies, to obtain

$$r_\mathrm{p} = \frac{R_\mathrm{j} u_\mathrm{j}}{U_\mathrm{T}\tan\theta_2}\left(\frac{q}{q_0}\right)^{-1/4}\sqrt{1+\frac{4}{3}\frac{qU_\mathrm{T}}{u_\mathrm{j}}} \tag{11.3}$$

and

$$f_m = \frac{\tan\theta_2}{4\pi R_\mathrm{j}}\sqrt{\frac{\gamma P_0 U_\mathrm{T}}{\rho_\mathrm{w}}}\, z_{\mu,m} q_0^{-1/4} q^{-1/4} u_\mathrm{j}^{-1/2}, \tag{11.4}$$

respectively. In these expressions, q_0 is an appropriate scaling factor and, obviously, when $q = q_0$, the eigenfrequencies predicted by (10.4) and (11.4) are identical.

The unknown factor q_0 can be determined from observations of the penetration depth, r_p, of the plume. Using a photographic technique, r_p was measured as a function of jet velocity, u_j, with q held constant. The results are in accordance with both (11.3) and the observations of Clanet & Lasheras (1997) in that the penetration depth was found to vary linearly with u_j, as illustrated in figure 15*a* for $q = 0.55$. A least-squares fit of (11.3) to these data yields $q_0 = 0.25$. Figure 15*b* shows the

Table 1. *Values of parameters used in evaluating the void fraction and sound speed in the plume, the penetration depth and the eigenfrequencies*

parameter	value
R_j	0.8 mm
ρ_w	1000 kg m^{-3}
ρ_a	1 kg m^{-1}
K_w^{-1}	2.25 GPa
P_0	101.3 kPa
γ	1.3
q_0	0.25
θ_2	7.5°
U_T	0.24 m s^{-1}

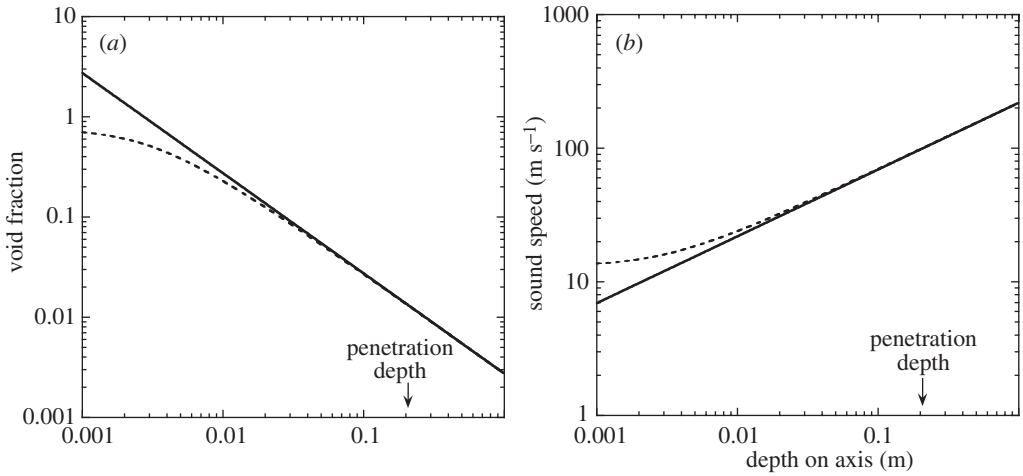

Figure 16. (*a*) Void-fraction profile from the exact (dashed line) and approximate (solid line) expressions in (6.5). (*b*) Sound-speed profile from (7.5) using the exact (dashed line) and approximate (solid line) forms of $\beta = \beta_x$ in (6.5). All curves were evaluated for $u_j = 9.5\,\mathrm{m\,s^{-1}}$ and $q = 0.55$.

measured penetration depth as a function of q for $u_j = 9.5\,\mathrm{m\,s^{-1}}$ and, for comparison, the theoretical expression in (11.3) with $q_0 = 0.25$. Note that the data in figure 15*b* become less reliable for $q < 0.5$.

In evaluating (11.3), the cone half-angle was set to $\theta_2 = 7.5°$. This angle, when substituted into the Gaussian expression for the void fraction in (5.2), accurately matches the data on the lateral spreading of the bubble plume in figure 31 of Bin (1993). Also needed was the terminal velocity, U_T, which, from figure 4 of Maxworthy *et al.* (1996), was taken as $U_T = 0.24\,\mathrm{m\,s^{-1}}$, appropriate to bubbles 4 mm in diameter, as found at the base of our freshwater plumes. The values of the remaining parameters used in evaluating the theoretical expressions are listed in table 1.

With the aid of these parameters, and using $(q/q_0)^{1/4}\tan\theta_2$ instead of $\tan\theta_2$, the void fraction and sound speed on the axis of the plume were computed from (6.5) and (7.5), respectively. Examples of the resultant profiles, for $u_j = 9.5\,\mathrm{m\,s^{-1}}$ and $q = 0.55$, are shown in figure 16. The void fraction decreases with depth, taking

Table 2. *Zeros of the function* $X_\mu(z_p) = z_p J'_\mu(z_p) - J_\mu(z_p)$

ν	μ	$z_{\mu,1}$	$z_{\mu,2}$	$z_{\mu,3}$	$z_{\mu,4}$	$z_{\mu,5}$	θ_f
1	3	3.6113	7.8693	11.2510	14.5142	17.7309	90.0
2	5	5.9624	10.3964	13.905	17.2498	20.5238	54.7
3	7	8.1904	12.8225	16.4555	19.8846	23.2208	39.2
4	9	10.3647	15.1862	18.9367	22.4484	25.8473	30.6
2.7	6.4	7.5293	12.1024	15.6988	19.1027	22.4200	42.9

values throughout most of the plume in the interval $0.2 \geqslant \beta_x \geqslant 0.01$, where the approximation in (6.5) is valid. Correspondingly, the sound speed increases with depth, but, even at the base of the plume, is at least an order of magnitude less than the sound speed in the surrounding water.

12. The zeros of X_μ

As noted earlier, to evaluate the predicted eigenfrequencies, it is necessary to know the zeros, $z_{\mu,m}$, of the function X_μ. These zeros depend on the value of μ, the order of the Bessel functions in (10.1), but μ itself is still unspecified. From the simple relationship in (9.10), it is evident that to determine μ we need to evaluate the degree, ν, of the Legendre function in the expression for the field in (9.7). This is achieved by finding the set of zeros of X_μ that provides the best fit between the predicted eigenfrequencies in (11.4) and the data in figures 7 and 8.

In table 2, the first five zeros of X_μ are listed for $\mu = 3, 5, 7, 9$, corresponding to Legendre functions of degree $\nu = 1, 2, 3, 4$. For each value of ν, the non-uniformly distributed zeros represent the first five longitudinal modes of the bubble-plume cavity. Of course, ν, representing the lowest-order angular mode, need not necessarily be integer. The best fit to the eigenfrequency data is obtained with $\mu = 6.4$ corresponding to $\nu = 2.7$, which yields zeros of X_μ, as shown on the last line of table 2. From (9.11), the first zero of the Legendre function of degree $\nu = 2.7$ gives the half-angle of the effective pressure-release cone as $\theta_f = 42.9°$.

Using the zeros for $\nu = 2.7$, the first five eigenfrequencies computed from (11.3) are plotted in figure 17 as a function of jet velocity, u_j, with the entrainment ratio held constant at $q = 0.55$. All five theoretical modes show good agreement with the data. The fit is of a similar quality in figure 18, which shows the theoretical eigenfrequencies as a function of q with the jet velocity held constant at $u_\mathrm{j} = 9.5\,\mathrm{m\,s^{-1}}$. Note that if (10.4), without the empirical, q-scaling modification to $\tan\theta_2$, had been used instead of (11.4), the theoretical curves in figure 18 would have shown a slightly steeper negative slope than the data.

From the agreement between the theory and the data in figures 17 and 18, it may be inferred that the spectral peaks observed in the external acoustic field are driven by the first five longitudinal modes associated with the Legendre function of degree $\nu = 2.7$. Although smaller values of ν are possible, representing lower frequencies, the corresponding spectral peaks are not seen in the data, indicating that $\nu = 2.7$ does indeed represent the lowest-order angular mode of the bubble-plume cavity. In principle, the bubble plume could support higher-order angular modes, with values of ν satisfying (9.11). However, such high-frequency resonances are not seen in the data,

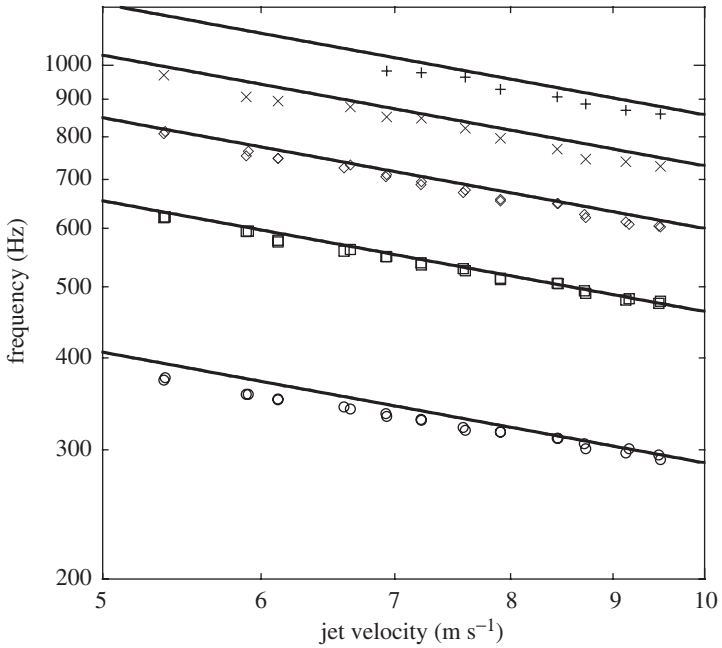

Figure 17. The first five eigenfrequencies versus jet velocity, with constant $q = 0.55$. The solid lines were computed from (11.3) using the zeros in table 2 corresponding to $v = 2.7$. The symbols represent the same data as shown in figure 8.

indicating that, if present at all, either they are suppressed by the high attenuation in the bubble plume or they occur above our upper frequency limit of 1 kHz.

13. Concluding remarks

The sound-pressure field emanating from the conical bubble plume formed in a pool of fresh water by a vertical freshwater plunging jet exhibits clearly defined spectral peaks, which are non-uniformly spaced in frequency between 100 Hz and 1 kHz. Each of the eigenfrequencies scales as $u_{\mathrm{j}}^{-1/2} q^{-1/4}$, where u_{j} is the jet velocity and q is the air entrainment ratio. A theoretical model has been developed in which the biphasic bubble plume is treated as a continuum that acts as an acoustically leaky resonant conical cavity. In effect, the bubbles undergo coherent collective oscillations, that is, the bubble-plume rings, with resonances that are governed by the conical geometry of, and the sound-speed structure within, the plume.

An argument based on the conservation of downward momentum flux leads to a sound-speed profile within the bubble plume of the form $c \propto r^{1/2}$, where r is radial distance from the penetration point of the jet. A solution of the wave equation for the field in a plume with this square-root profile yields longitudinal resonances at frequencies that scale as $u_{\mathrm{j}}^{-1/2}$, as seen in the data. In contradistinction, a uniform profile would give rise to eigenfrequencies that scale incorrectly as u_{j}^{-1}. It has previously been recognized that the sound-speed profile within an ocean bubble layer may form a waveguide that significantly influences acoustic transmission through the layer (Buckingham 1991; Farmer & Vagle 1989); and it is also known that the bubble cloud formed beneath a breaking wave exhibits a non-uniform void fraction and an

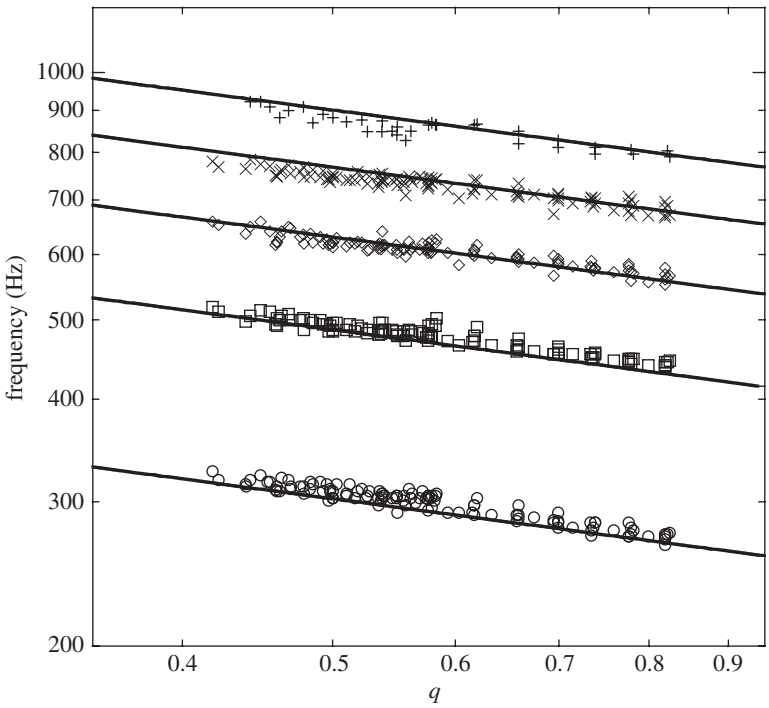

Figure 18. The first five eigenfrequencies versus air entrainment ratio, with $u_j = 9.5\,\mathrm{m\,s^{-1}}$ constant. The solid lines were computed from (11.3) using the zeros in table 2 corresponding to $v = 2.7$. The symbols represent the same data as shown in figure 7.

associated sound-speed distribution (Lamarre & Melville 1994). It has not, however, been widely appreciated that the spectral properties of the external acoustic field may depend strongly on the internal sound-speed structure of the bubble plume.

The resonant character of the bubble plume is relevant to questions concerning the mechanisms underlying low-frequency (less than 1 kHz) wind-generated ambient noise in the ocean. Of course, our laboratory jets differed in several respects from the natural jets that are associated with wave breaking on the ocean surface. Obviously, sea water is saline, whereas the experiments reported in this article were conducted with freshwater. In the former, the bubbles are significantly smaller, which influences the penetration depth of the plume and, in turn, the longitudinal resonances. Another difference is that natural jets do not generally penetrate at normal incidence to the sea surface, which is likely to lead to a deformed plume with resonance properties differing from those of the axisymmetric conical plume produced by a vertical jet. Finally, and perhaps more importantly, a typical ocean jet is a transient phenomenon with a lifetime of order 1 s, whereas our jets played continuously. Little is known of the acoustic properties of a bubble plume formed by a transient jet, but one interesting issue concerns the time taken by the plume and its associated sound field to become fully established. If the formation time of the plume were significantly shorter than the lifetime of the jet, then the plume may act as a resonant cavity in much the same way as observed with a continuous jet. If the reverse were true, then presumably the plume would never reach a fully developed state, in which case resonance peaks would not be expected in the spectrum of the external sound field.

We are indebted to Professor Juan Lasheras for his advice and encouragement during the formative stages of our experiments. This work was supported by the US Office of Naval Research, Ocean Acoustics Code (Dr J. Simmen) under grant numbers N00014-93-1-0054 and N00014-00-1-0050.

Appendix A. Green's function for the conical cavity

The field in the bubble plume is obtained from the solution of (9.5),

$$\frac{\partial^2 w}{\partial z^2} + \frac{1}{z}\frac{\partial w}{\partial z} - \frac{w}{z^2} + \frac{4}{z^2 \sin\theta}\frac{\partial}{\partial \theta}\left(\sin\theta \frac{\partial w}{\partial \theta}\right) + w = -s\frac{8\omega}{\alpha}\frac{\delta(z^2 - z'^2)\delta(\theta)}{z\sin\theta}. \quad (A\,1)$$

This equation is separable and may be solved by applying Legendre and Hankel transformations to both sides.

The appropriate Legendre transform is taken over the half-angle of the effective cone,

$$w_{\nu_i} = \int_0^{\theta_f} w P_{\nu_i}(\cos\theta)\sin\theta\,\mathrm{d}\theta, \quad (A\,2)$$

the inverse of which is

$$w = \sum_{i=1}^{\infty} A_{\nu_i} w_{\nu_i} P_{\nu_i}(\cos\theta), \quad (A\,3)$$

where $P_\nu(\cos\theta)$ is the Legendre function of the first kind of degree ν and the normalizing coefficient is

$$A_{\nu_i} = \left\{\int_0^{\theta_f} P^2_{\nu_i}(\cos\theta)\sin\theta\,\mathrm{d}\theta\right\}^{-1}. \quad (A\,4)$$

The summation in (A 3) is taken over all allowed values of $\nu = \nu_i$, $i = 1, 2, \ldots$. These values are the real zeros of $P_\nu(\cos\theta)$, that is, the roots of the equation representing the pressure-release boundary condition on the flanks of the effective cone,

$$P_\nu(\cos\theta_f) = 0. \quad (A\,5)$$

It is implicit in (A 2) and (A 3) that the Legendre functions of degree ν_i are orthogonal on the interval $[0, \theta_f]$, which may be proved using an argument analogous to that for the orthogonality of the Legendre polynomials on the interval $[0, \pi]$ (Lebedev 1965). On integrating by parts twice, the Legendre transform of the second derivative with respect to polar angle, θ, is readily shown to be

$$\int_0^{\theta_f} \frac{1}{\sin\theta}\frac{\partial}{\partial\theta}\left(\sin\theta\frac{\partial w}{\partial\theta}\right) P_{\nu_i}(\cos\theta)\sin\theta\,\mathrm{d}\theta = -\nu_i(\nu_i+1)w_{\nu_i}, \quad (A\,6)$$

and thus the Legendre transformed version of (A 1) is

$$\frac{\partial^2 w_{\nu_i}}{\partial z^2} + \frac{1}{z}\frac{\partial w_{\nu_i}}{\partial z} - \mu_i^2\frac{w_{\nu_i}}{z^2} + w_{\nu_i} = -\frac{8sb^{1/2}}{z}\delta(z^2 - z'^2). \quad (A\,7)$$

Equation (A 7) is Bessel's (inhomogeneous) equation of order $\mu_i = (2\nu_i + 1)$, which may be solved using standard techniques based on the finite Hankel transform, defined as

$$w_{\nu_i,p} = \int_0^{z_p} z w_{\nu_i}(z) J_{\mu_i}(pz)\,\mathrm{d}z, \quad (A\,8)$$

where $J_\mu(\cdot)$ is the Bessel function of the first kind of order μ and z_p is defined in (9.8) in terms of the penetration depth of the bubble plume. The inverse Hankel transform is

$$w_{\nu_i} = \int_0^\infty p w_{\nu_i,p} J_{\mu_i}(pz)\,\mathrm{d}p, \tag{A 9}$$

and the finite transform of the first three terms on the left-hand side of (A 7) is

$$\int_0^{z_p} z\Delta_{\nu_i}(z) J_{\mu_i}(pz)\,\mathrm{d}z = -p^2 w_{\nu_i,p} + z_p w'_{\nu_i}(z_p) J_{\mu_i}(pz_p) - z_p w_{\nu_i}(z_p) J'_{\mu_i}(pz_p), \tag{A 10}$$

where the primes denote differentiation with respect to the argument and

$$\Delta_{\nu_i}(z) \equiv \frac{\partial^2 w_{\nu_i}}{\partial z^2} + \frac{1}{z}\frac{\partial w_{\nu_i}}{\partial z} - \mu_i^2 \frac{w_{\nu_i}}{z^2}. \tag{A 11}$$

On applying these results to (A 7), the transformed field is found to be

$$w_{\nu_i,p} = \frac{-z_p w'_{\nu_i}(z_p) J_{\mu_i}(pz_p) + z_p w_{\nu_i}(z_p) J'_{\mu_i}(pz_p) - 4b^{1/2} s z'^{-1} J_{\mu_i}(pz')}{(1-p^2)}. \tag{A 12}$$

From (A 9), the inverse-transform of this expression yields the result

$$w_{\nu_i}(z) = -j\frac{\pi}{2}\Bigg[z_p w_{\nu_i}(z_p) J_{\mu_i}(z) H^{(1)\prime}_{\mu_i}(z_p) - z_p w'_{\nu_i}(z_p) J_{\mu_i}(z) H^{(1)}_{\mu_i}(z_p) - 4b^{1/2} s \frac{J_{\mu_i}(z')}{z'} H^{(1)}_{\mu_i}(z)\Bigg], \tag{A 13}$$

which has been obtained with the aid of Hankel's discontinuous integral (Watson 1958),

$$\int_0^\infty \frac{p}{p^2-a^2} J_\mu(pz_1) J_\mu(pz_2)\,\mathrm{d}p = \tfrac{1}{2}\pi j J_\mu(az_1) H^{(1)}_\mu(az_2) \quad \text{for } z_2 > z_1. \tag{A 14}$$

The constants of integration, $w_{\nu_i}(z_p)$ and $w'_{\nu_i}(z_\mathrm{p})$, in (A 13) are determined using the rigid boundary condition at the base of the cone. This leads to the relationship

$$w'_{\nu_i}(z_p) = \frac{w_{\nu_i}(z_p)}{z_p} \tag{A 15}$$

which, when substituted into (A 13), yields

$$w_{\nu_i}(z_b) = 4b^{1/2} s \frac{J_{\mu_i}(z')}{z'} \frac{1}{z_p J'_{\mu_i}(z_p) - J_{\mu_i}(z_p)}. \tag{A 16}$$

It follows that the Legendre-transformed field is

$$w_{\nu_i}(z) = -2\pi s \frac{\omega}{\alpha} \frac{J_{\mu_i}(z')}{z'} \frac{1}{[z_\mathrm{p} J'_{\mu_i}(z_\mathrm{p}) - J_{\mu_i}(z_\mathrm{p})]} F_i(z, z_\mathrm{p}), \tag{A 17}$$

where

$$F_i(z, z_\mathrm{p}) = J_{\mu_i}(z)[Y_{\mu_i}(z_\mathrm{p}) - z_\mathrm{p} Y'_{\mu_i}(z_\mathrm{p})] + Y_{\mu_i}(z)[z_\mathrm{p} J'_{\mu_i}(z_\mathrm{p}) - J_{\mu_i}(z_\mathrm{p})]. \tag{A 18}$$

The full angular dependence of the field is obtained by substituting (A 17) into the modal expansion in (A 3),

$$w(z,\theta) = -\frac{2\pi s}{z'}\frac{\omega}{\alpha}\sum_{i=1}^{\infty} A_{\nu_i}\frac{J_{\mu_i}(z')}{[z_{\rm p}J'_{\mu_i}(z_{\rm p}) - J_{\mu_i}(z_{\rm p})]}F_i(z,z_{\rm p})P_{\nu_i}(\cos\theta). \tag{A 19}$$

It is now, finally, a straightforward matter to derive the solution for the velocity potential, $\psi(r,\theta)$, from (9.3) and (9.4).

The full expression for the field is not, however, necessary in order to determine the eigenfrequencies. These are obtained from the poles of (A 16) or (A 17), which correspond to the zeros of the term in square brackets in the denominators of these expressions. The properties of these zeros and their relationship to the eigenfrequencies are discussed in the text.

References

Berger, T. K. 1999 Hydrodynamic properties of air entraining flows: a study using new acoustic techniques, p. 128. PhD thesis, University of California, San Diego, CA, USA.

Berger, T. K., Hahn, T. R. & Buckingham, M. J. 2003 Theory and experiments on the depth of penetration of bubbles entrained by a plunging jet in fresh and salt water. *J. Fluid Mech.* (In preparation.)

Bin, A. K. 1976 Investigation of the aeration effect of a free liquid jet. PhD thesis, Warsaw University of Technology, Warsaw, Poland.

Bin, A. K. 1988 Minimum air entrainment velocity of vertical plunging liquid jets. *Chem. Engng Sci.* **43**, 379–389.

Bin, A. K. 1993 Gas entrainment by plunging liquid jets. *Chem. Engng Sci.* **48**, 3585–3630.

Buckingham, M. J. 1979 Array gain of a broadside vertical line array in shallow water. *J. Acoust. Soc. Am.* **65**, 148–161.

Buckingham, M. J. 1987 Theory of three-dimensional acoustic propagation in a wedge-like ocean with a penetrable bottom. *J. Acoust. Soc. Am.* **82**, 198–210.

Buckingham, M. J. 1991 On acoustic transmission in ocean-surface waveguides. *Phil. Trans. R. Soc. Lond.* A **335**, 513–555.

Burgess, A. S. & Kewley, D. J. 1983 Wind-generated surface noise source levels in deep water east of Australia. *J. Acoust. Soc. Am.* **83**, 201–210.

Carey, W. M. & Bradley, M. P. 1985 Low-frequency ocean surface noise sources. *J. Acoust. Soc. Am. Suppl.* **78**, S1–S2.

Carey, W. M. & Fitzgerald, J. W. 1987 Low-frequency noise and bubble plume oscillations. *J. Acoust. Soc. Am. Suppl.* **82**, S62.

Carey, W. M. & Browning, D. 1988 Low frequency ocean ambient noise: measurements and theory. In *Sea surface sound: natural mechanisms of surface generated noise in the ocean* (ed. B. R. Kerman), pp. 361–376. Dordrecht: Kluwer.

Carey, W. M., Fitzgerald, J. W., Monahan, E. C. & Wang, Q. 1993 Measurement of the sound produced by a tipping trough with fresh and salt water. *J. Acoust. Soc. Am.* **93**, 3178–3192.

Carstensen, E. L. & Foldy, L. L. 1947 Propagation of sound through a liquid containing bubbles. *J. Acoust. Soc. Am.* **19**, 481–501.

Clanet, C. & Lasheras, J. C. 1997 Depth of penetration of bubbles entrained by a plunging water jet. *Phys. Fluids* **9**, 1864–1866.

Evans, G. M. 1990 A study of a plunging jet bubble column. PhD thesis, University of Newcastle, Newcastle, UK.

Evans, G. M., Jameson, G. J. & Atkinson, B. W. 1992 Prediction of the bubble size generated by a plunging liquid jet bubble column. *Chem. Engng Sci.* **47**, 3265–3272.

Farmer, D. M. & Vagle, S. 1989 Waveguide propagation of ambient sound in the ocean-surface bubble layer. *J. Acoust. Soc. Am.* **86**, 1897–1908.

Feuillade, C. 1996 The attenuation and dispersion of sound in water containing multiply interacting air bubbles. *J. Acoust. Soc. Am.* **96**, 3412–3430.

Foldy, L. L. 1945 The multiple scattering of waves. I. General theory of isotropic scattering by randomly distributed scatterers. *Phys. Rev.* **67**, 107–119.

Hahn, T. R. 1999 Low-frequency acoustic emissions of a plunging water jet, p. 130. PhD thesis, University of California, San Diego, CA.

Hinze, J. O. 1975 *Turbulence*, 2nd edn. McGraw-Hill.

Hollett, R. D. 1994 Observations of underwater sound at frequencies below 1500 Hz from breaking waves at sea. *J. Acoust. Soc. Am.* **95**, 165–170.

Karplus, H. B. 1958 The velocity of sound in a liquid containing gas bubbles. Armour Research Foundation, University of Illinois Project c00–248, TID-4500.

Kerman, B. R. 1984 Underwater sound generation by breaking wind waves. *J. Acoust. Soc. Am.* **75**, 149–165.

Kolaini, A. R. 1998 Sound radiation by various types of laboratory breaking waves in fresh and salt water. *J. Acoust. Soc. Am.* **103**, 300–308.

Kolaini, A. R. & Crum, L. A. 1994 Observations of underwater sound from laboratory breaking waves and the implications concerning ambient noise in the ocean. *J. Acoust. Soc. Am.* **96**, 1755–1765.

Kolaini, A. R., Roy, R. A., Crum, L. A. & Mao, Y. 1993 Low-frequency underwater sound generation by impacting transient water jets. *J. Acoust. Soc. Am.* **94**, 2809–2820.

Lamarre, E. & Melville, W. K. 1994 Void-fraction measurements and sound-speed fields in bubble plumes generated by breaking waves. *J. Acoust. Soc. Am.* **95**, 1317–1328.

Lebedev, N. N. 1965 *Special functions and their applications*. Englewood Cliffs, NJ: Prentice-Hall.

Leighton, T. G. 1994 *The acoustic bubble*. Academic.

Loewen, M. R. & Melville, W. K. 1994 An experimental investigation of the collective oscillations of bubble plumes entrained by breaking waves. *J. Acoust. Soc. Am.* **95**, 1329–1343.

McKeogh, E. J. & Ervine, D. A. 1981 Air entrainment rate and diffusion pattern of plunging liquid jets. *Chem. Engng Sci.* **36**, 1161–1172.

Maxworthy, T., Gnann, C., Kürten, M. & Durst, F. 1996 Experiments on the rise of air bubbles in clean viscous liquids. *J. Fluid Mech.* **321**, 421–441.

Minnaert, M. 1933 On musical air-bubbles and the sounds of running water. *Phil. Mag.* **16**, 235–248.

Nicholas, M., Roy, R. A., Crum, L. A., Oguz, H. & Prosperetti, A. 1994 Sound emissions by a laboratory bubble cloud. *J. Acoust. Soc. Am.* **95**, 3171–3182.

Orris, G. & Nicholas, M. 2000 Collective oscillations of fresh and salt water bubble plumes. *J. Acoust. Soc. Am.* **107**, 771–787.

Prosperetti, A. 1988*a* Bubble-related ambient noise in the ocean. *J. Acoust. Soc. Am.* **84**, 1042–1054.

Prosperetti, A. 1988*b* Bubble dynamics in oceanic ambient noise. In *Natural mechanisms of surface generated noise in the ocean* (ed. B. R. Kerman), pp. 151–171. Dordrecht: Kluwer.

Smigelschi, O. & Suciu, G. D. 1976 Size of the submerged biphasic region in plunging jet systems. *Chem. Engng Sci.* **31**, 1217–1220.

Tennekes, H. & Lumley, J. L. 1972 *A first course in turbulence*. Cambridge, MA: MIT Press.

Townsend, A. A. 1976 *The structure of turbulent shear flows*, 2nd edn. Cambridge University Press.

Urick, J. R. 1986 *Ambient noise in the sea*. Los Altos, CA: Peninsula.

van de Donk, J. A. C. 1981 Water aeration with plunging jets. PhD thesis, Technische Hogeschool Delft.

van de Sande, E. 1974 Air entrainment by plunging water jets. PhD thesis, Technische Hogeschool Delft.

van de Sande, E. & Smith, J. M. 1973 Surface entrainment of air by high velocity water jets. *Chem. Engng Sci.* **28**, 1161–1168.

van de Sande, E. & Smith, J. M. 1975 Mass transfer from plunging water jets. *Chem. Engng J.* **10**, 225–233.

Watson, G. N. 1958 *A treatise on the theory of Bessel functions*, 2nd edn. Cambridge University Press.

Weston, D. E. 1960 A Moiré fringe analog of sound propagation in shallow water. *J. Acoust. Soc. Am.* **32**, 647–654.

Wille, P. C. & Geyer, D. 1984 Measurements on the origin of the wind dependent ambient noise variability in shallow water. *J. Acoust. Soc. Am.* **75**, 173.

Wood, A. B. 1964 *A textbook of sound*, 3rd edn. London: G. Bell and Sons.

Wygnanski, I. & Fiedler, H. 1969 Some measurements in the self-preserving jet. *J. Fluid Mech.* **38**, 577–612.

Yoon, S. W., Crum, L. A., Prosperetti, A. & Lu, N. Q. 1991 An investigation of the collective oscillations of a bubble cloud. *J. Acoust. Soc. Am.* **89**, 700–706.